Characterising Pavement Surface Damage Caused by Tyre Scuffing Forces

Neon Taramoeroa
John de Pont
TERNZ Ltd, Auckland

Land Transport New Zealand Research Report 347

ISBN 978-0-478-30974-4
ISSN 1177-0600

PO Box 2840, 44 Victoria St, Wellington, New Zealand
Telephone 64-4 894 5400; Facsimile 64-4 894 6100
Email: *research@landtransport.govt.nz*
Website: *www.landtransport.govt.nz*

Taramoeroa, N., de Pont, J. 2008. Characterising pavement surface damage caused by tyre scuffing forces. *Land Transport New Zealand Research Report 374.* 66 pp.

Transport Engineering Research New Zealand (TERNZ) Ltd,
PO Box 97 846, South Auckland Mail Centre, Manakau City 1702
Auckland, New Zealand

Keywords: directional performance, dual tyres, lateral load transfer, multi-axle groups, pavement scuffing, self-steering axles, tyre scrubbing, tyre scuffing, wide-single tyres

An important note for the reader

Land Transport New Zealand is a crown entity established under the Land Transport Management Act 2003. The objective of Land Transport New Zealand is to allocate resources and undertake its functions in a way that contributes to an integrated, safe, responsive and sustainable land transport system. Each year, Land Transport New Zealand invests a portion of its funds on research that contributes to this objective.

The research detailed in this report was commissioned by Land Transport New Zealand.

While this report is believed to be correct at the time of its preparation, Land Transport New Zealand, and its employees and agents involved in its preparation and publication, cannot accept any liability for its contents or for any consequences arising from its use. People using the contents of the document, whether directly or indirectly, should apply and rely on their own skill and judgement. They should not rely on its contents in isolation from other sources of advice and information. If necessary, they should seek appropriate legal or other expert advice in relation to their own circumstances, and to the use of this report.

The material contained in this report is the output of research and should not be construed in any way as policy adopted by Land Transport New Zealand but may be used in the formulation of future policy.

Acknowledgments

TERNZ Ltd thanks Kerry Arnold from the Road Transport Forum NZ, Don Hutchinson from Land Transport NZ, Dom Kalasih from the Ministry of Transport NZ, Kieran Sharp from ARRB Group Ltd, and Lynn Sleath from Transit NZ for their time and expertise. TERNZ also thanks Rod Mackay from Optimech Services for his assistance with the field trial data acquisition, and thanks Kaye Clark from the Waikato District Council for the use of the field trial venue. Their assistance was critical to the success of this research.

The steering group for this report was comprised of Kerry Arnold, Don Hutchinson, Dom Kalasih and Lynn Sleath. The peer reviewers were Dom Kalasih and Kieran Sharp and Lynn Sleath.

Abbreviations and acronyms

CG	Centre of Gravity
GVM	Gross Vehicle Mass
LTNZ	Land Transport New Zealand
LTSA	Land Transport Safety Authority of New Zealand, now LTNZ
SAE	Society of Automotive Engineers
TAC	Tyre-Axle-Coupling sequence
VDM Rule	Vehicle Dimensions and Mass 2002 – Rule 41001

Contents

Executive summary

Introduction

Over time, the size and weight of heavy vehicles has gradually increased. As weight increases, pavement wear also increases. This is a concern for road controlling authorities who need to manage this and provide a serviceable network for their users. The management of pavement wear has primarily focused on the distress caused by vertical loads. This includes cracking, rutting and roughness. One of the ways of reducing the impact of vertical loading is to increase the number of axles and so we have seen an evolution from single axles to tandem, tridem (tri-axle), and, in some jurisdictions, quadem axle (quad-axle) groups. Multi-axle groups reduce the peak vertical loading and, when closely spaced, reduce the magnitude of the strain cycles to which the pavement is subjected. However, where tight low-speed turns are executed, non-steering axle groups lead to transverse shear forces at the pavement–tyre interface.

In New Zealand, the most widely used pavement construction is an unbound granular structure with chipseal surfacing. Asphaltic concrete is used on the more heavily trafficked sections of pavement, including parts of the State Highway network. With asphaltic concrete pavements, tensile shear stresses from tyres can cause surface cracking and ravelling. Thus, the increased use of non-steering axle groups is likely to result in increased pavement wear in the vicinity of intersections and roundabouts where tight low-speed turns are executed. Recent research suggests that the damage to chipseal surfaces increases in proportion to the maximum tensile strain raised to the fifth power. In New Zealand, concern over these pavement damage effects has resulted in regulators requiring quad-axle groups to be fitted with two self-steering axles. In cases where self-steering axles are used, this has been stated explicitly; otherwise, it is assumed that all axles in the group are non-steering axles. In addition, all axle groups are assumed to be multi-axle groups unless otherwise stated.

Methodology

The magnitude of the transverse shear forces generated by multi-axle groups depends on many factors including:

- turn geometry,
- the type of vehicle,
- axle weights,
- tyre size and configuration,
- suspension geometry and compliance, and
- the number of non-steering, self-steering, and actively steered axles.

This study quantifies the impact of some of these parameters on the magnitude of the transverse pavement shear forces or scuffing forces generated during constant low-speed turns. This had two main parts:

1. A field trial was undertaken to assess the level of scuffing force required to cause visible wear on the pavement surface and to validate the computer simulation software. The physical testing was done on a section of road that was formerly part of State Highway 1 but is now a local access road. The pavement construction was

an unbound granular structure with chipseal surfacing. For this test, a three-axle full-trailer with a single-axle dolly was jack-knifed. The drawbar was towed at a constant crawl speed perpendicular to the trailer's alignment, and the towing force was measured. This manoeuvre was repeated for different tandem axle group loads. A similarly configured computer model of a tandem simple-trailer was used to simulate the forces observed in the field trial.

2. Computer models of a tandem and tridem simple-trailer were used to assess the effects of axle load, axle group spread, wheelbase, and turn geometry on peak scuffing forces. Computer models for typical heavy vehicle configurations currently used in New Zealand were used to simulate various low-speed turns and the relative impact of the peak scuffing forces for the different vehicles were determined. The key vehicle and turn parameters that affect the magnitude of the scuffing forces were identified.

The inter-relationship between scuffing forces, directional stability, lateral load transfer, and rollover stability is also considered.

Findings

- Axle groups with self-steering axles generate less scuffing forces than comparable non-steering axle groups. For tight turns, however, these axles can reach their steer angle limits, at which point they respond like non-steering axles and thus giving rise to an increase in scuffing forces.
- For the same axle group weight and axle group spread, wide-single tyres generate higher scuffing forces than dual tyres.
- Scuffing forces increase with increasing axle group spread.
- When laden to the maximum legal weight limits, tridem axle groups produced higher scuffing forces than tandem axle groups even though the tridem axle groups have less weight per axle.
- Scuffing forces decrease with increasing turn radius.
- For vehicles without self-steering axles, the highest steady-state scuffing forces are generated by tractor semi-trailers followed by B-trains, then truck and full-trailers, and then single-unit trucks.
- Even during low-speed turns with minimal lateral acceleration, significant lateral load transfer can occur from having an elevated roll centre, thus leading to higher peak vertical loads. Higher peak scuffing forces result than would be the case if load transfer did not occur. Lateral load transfer caused by body roll can also be induced by tow coupling forces applied at a vertical distance offset from the roll centre, but this effect is only significant for large articulation angles. No lateral load transfer caused by body roll will occur if the tow coupling is at the same height as the roll centre of the suspension.
- For small angles of turn (90^o or less), shorter wheelbase single-unit vehicles generate higher scuffing forces than comparable vehicles with longer wheelbases, but the reverse is true for large turn angles as these vehicles approach steady-state.

- For a given turn radius, the axle group on which the peak scuffing forces occur can change as the turn angle increases. If a change occurs, in general, the critical axle group then shifts backward through the vehicle's more widely spread axle groups, although not necessarily in succession. The peak scuffing force generally occurs on the tyres of the lead non-steering axle within the axle group.
- Minor visible abrasion of the chipseal surface was observed in the field trial at the lowest gross tandem axle group load (a little under 7 tonnes). Small fragments approximately 1 mm in diameter were broken off the exposed corners of the chip. The corresponding peak scuffing force is 9% more than that calculated for the legally configured tridem semi-trailer undergoing the 13.75 m radius 360^{o} turn. This latter manoeuvre is less severe than the 25 m wall-to-wall 360^{o} turn capability required by the Vehicle Dimensions and Mass Rule.

Conclusions

It is clear from the study that reducing axle weight, axle group spread, and road curvature (increasing turn radius) reduces scuffing forces and their impact on pavement wear. The amount of scuffing force also depends on the tyre configuration, the use of self-steering axles, and on the type of vehicle.

Our findings also validated the general rule found in other research: measures taken to improve low-speed performance reduce high-speed performance, and vice versa. For example, wide-single tyres produce higher scuffing forces than dual tyres. However, the use of wide-single tyres increases the tyre track widths, which can slightly improve rollover stability. The use of self-steering axles results in lower scuffing forces, but the lower overall cornering stiffness reduces high-speed directional performance compared with similar non-steering axle groups. For vehicles without self-steering axles, the highest steady-state scuffing forces are generated by tractor semi-trailers, followed by B-trains, and then truck and full-trailers. This ranking of heavy vehicles is similar to that when ranked, in descending order, according to high-speed directional performance.

The tyre cornering stiffness, and therefore the amount of scuffing force, also depends on inflation pressure. In the case of truck tyres, the influence of inflation pressure on cornering stiffness varies and depends on obscure sensitivities to details in the carcass design. Thus the overall influence of inflation pressure on cornering stiffness cannot be generalised across all tyre types.

In general, the pavement wear resulting from scuffing forces will depend on many factors including the overall pavement design, the condition of the pavement, and various environmental factors.

Recommendations

- When designing intersections and roundabouts, the turn radius should be as large as possible. This will lead to reduced scuffing forces.
- Where tight radius turns are unavoidable, the pavement surface design should take into account the high level of scuffing forces that will occur.
- Research should be undertaken to determine whether the weight limits on tridem and quad-axle groups should vary with dual or wide-single tyre configurations. The Vehicle Dimensions and Mass Rule (VDM Rule) allows for tandem axle groups to carry more weight when configured with dual tyres than they could with wide-single tyres. The VDM Rule for tridem and quad-axle groups permits the same axle weight limit regardless of tyre configuration.
- Research should be undertaken to investigate whether a pavement scuffing force damage component should be incorporated into the Road User Charges Cost Allocation Model. The current Cost Allocation Model accounts for the pavement wear caused by vertical loads but does not account for the impact of pavement scuffing forces on pavement wear for a given vehicle configuration.

Abstract

The transverse shear forces generated by multi-axle groups depends on many factors including turn geometry, vehicle type, axle weights, tyre size and configuration, suspension geometry, and the number and type of axles. This study quantifies the impact of some of these parameters on the transverse pavement shear forces or scuffing forces generated during constant low-speed turns.

- A field trial on an unbound granular pavement structure with chipseal surfacing assessed the level of scuffing force that caused visible wear on the pavement surface. A computer model of a tandem simple-trailer was used to simulate the forces observed in the field.
- Computer models were used to assess the effects of axle load, axle group spread, wheelbase, and turn geometry on peak scuffing forces; to simulate various low-speed turns; and to identify the relative impact of the peak scuffing forces for the different vehicles.

This study provides data on the level of peak scuffing forces generated by heavy vehicles in New Zealand, the inter-relationship between scuffing forces, directional stability, lateral load transfer, and rollover stability. This is fundamental to vehicle size and weight regulation, and to the design of pavements and turn geometry at intersections.

1. Introduction

1.1 Background

Over time, the size and weight of heavy vehicles has gradually increased. As weight increases, pavement wear also increases. This is a concern for road controlling authorities who need to manage this and provide a serviceable network for their users. The management of pavement wear has primarily focused on the distress caused by vertical loads, such as cracking, rutting, and roughness. One of the ways of reducing the impact of vertical loading is to increase the number of axles, so we have seen an evolution from single axles to tandem, tridem (tri-axle), and, in some jurisdictions, quadem (quad-axle) axle groups. Multi-axle groups reduce the peak vertical loading and, when closely spaced, reduce the magnitude of the strain cycles to which the pavement is subjected. However, where tight low-speed turns are executed, non-steering axle groups lead to transverse shear forces at the pavement–tyre interface.

In New Zealand, the most widely used pavement construction is an unbound granular structure with chipseal surfacing. Asphaltic concrete is used on more heavily trafficked sections of pavement, including parts of the State Highway network. With asphaltic concrete pavements, tensile shear stresses from tyres can cause surface cracking and ravelling (Jacobs & Moraal 1992). Thus, the increased use of non-steering axle groups is likely to result in increased pavement wear in the vicinity of intersections and round-abouts where tight low-speed turns are executed. Recent research suggests that the damage to chipseal surfaces increases in proportion to the maximum tensile strain raised to the fifth power (National Transport Commission 2006). In New Zealand, concern over these pavement damage effects has resulted in regulators requiring quad-axle groups to be fitted with two self-steering axles. In cases where self-steering axles are used, this has been stated explicitly; otherwise, it is assumed that all axles in the group are non-steering axles. In addition, all axle groups are assumed to be multi-axle groups unless otherwise stated.

The pavement scuffing force is the horizontal shear force that reacts to the applied tyre scrubbing force. This study focuses on the magnitude of the transverse pavement scuffing forces or tyre cornering forces generated by vehicles with multi-axle groups undergoing constant low-speed turns over a horizontal pavement with uniform friction characteristics.

For convenience, in this report, the vertical force per tyre group (dual, single, or wide-single tyres) shall be referred to as the vertical force, vertical load, or weight. Similarly, the transverse scrubbing force per tyre group shall be referred to as the scrubbing force. The transverse pavement scuffing force per tyre group shall be referred to as the scuffing force or cornering force. The force of friction is considered when shear forces between the pavement–tyre interfaces are discussed. The scrubbing force and scuffing force are equal in magnitude but act in the opposite direction to each other. However, this study focuses on the magnitude of these transverse forces, so they are generally referred to in absolute

terms. The use of either of these forces depends on the frame of reference (pavement–tyre interface, body-fixed or world co-ordinates) and on the context of the discussion. The magnitude of the slip angle per tyre group is referred to as the slip angle or slip.

1.3 Structure

This report has been structured as follows:

- Chapter 2 presents some background theory and describes the simulation software used in the study.
- Chapter 3 presents the results of the field trial.
- Chapter 4 outlines the computer simulation study.
- Chapter 5 presents the results of the computer simulation study.
- Chapter 6 discusses the findings in the previous chapters.
- Chapter 7 presents the conclusions and recommendations.

Details of all the relevant vehicle parameters used in the simulation models are given in Appendix A. Appendix B gives performance maps for the tandem and tridem simple-trailers. A glossary of the terms used in the equations and the performance maps are listed in Appendix C.

2. Background

2.1 Cornering force

2.1.1 Overview

When a rolling pneumatic tyre is oriented in line with its direction of travel, the cornering force is zero. When the tyre is subjected to a transverse force, an angle is created between the direction of the tyre heading and the direction of travel. This angle is known as the slip angle. For small angles of slip, the cornering force increases linearly with slip angle. For larger slip angles, the cornering force increases nonlinearly with slip angle at a reducing rate. The cornering force also increases nonlinearly with vertical load at a reducing rate (see Figure 2.1).

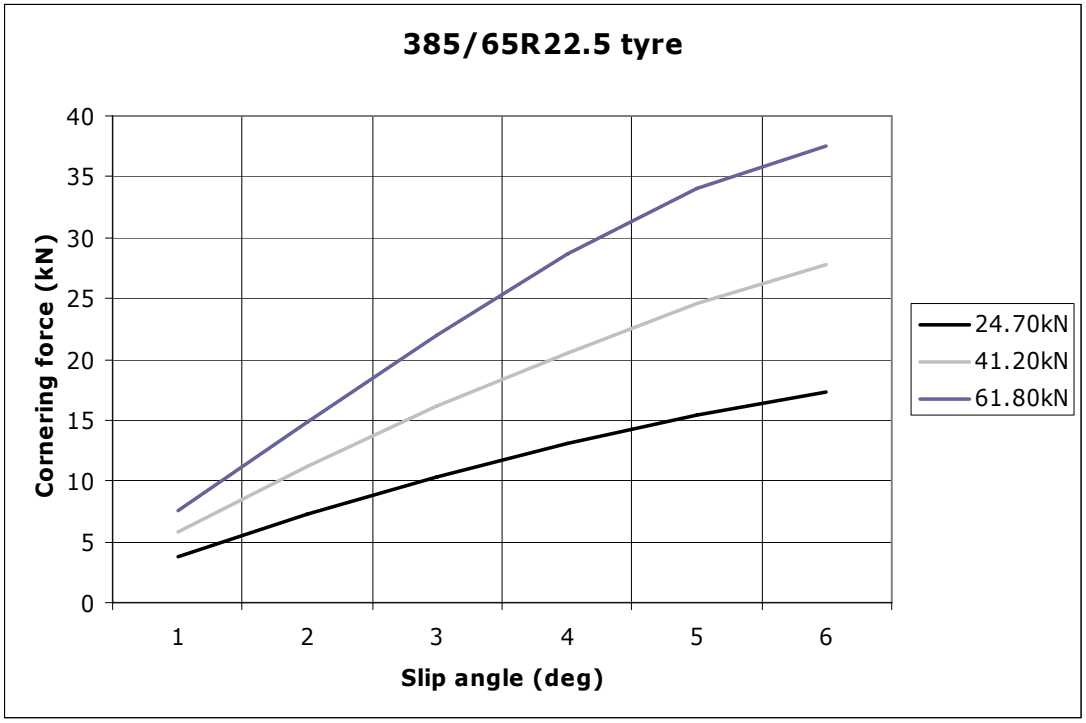

Figure 2.1 Relationship between cornering force and slip angle by vertical load for 385/65R22.5 tyres (taken from tyre manufacturers' data sheets and unpublished data from the University of Michigan Transportation Institute).

A property of primary importance regarding the directional behaviour of a vehicle is the cornering stiffness. The Society of Automotive Engineers (SAE) (Gillespie 1992) defines cornering stiffness as:

> *The negative of the slope of the transverse force versus slip angle curve evaluated at zero slip angle, where a positive slip angle produces a negative cornering force on the tyre*

The cornering stiffness also increases nonlinearly with vertical load at a reducing rate[1]. Other variables that influence cornering stiffness include tyre inflation pressure, profile, and width (Gillespie 1992). Since inflation pressure increases vertical stiffness but changes contact area, the overall influence on cornering stiffness cannot be generalised across all tyre types. It is generally accepted that increasing inflation pressure results in increasing cornering stiffness for passenger car tyres. In the case of truck tyres, the influence of inflation pressure on cornering stiffness is varied and dependent on obscure sensitivities to details in the carcass design. Inflation pressure has the most influence on cornering force production at high vertical loads, and tyres at reduced inflation pressures arrive at cornering force saturation at substantially higher values of slip angle. The profile of a tyre is expressed as a percentage of section height to section width. For the same overall tyre height, increasing the tyre width or rim diameter will lower the profile of the tyre. Lower profile tyres generally have greater cornering stiffness. Increasing cornering stiffness is likely to increase scuffing force but can improve high-speed directional performance.

The cornering force builds up as the tread elements move backward in the contact patch up to a point where the cornering force acting on the element overcomes the friction available, and slip occurs (Gillespie 1992). The simplified profile of the cornering force developed throughout the contact patch takes the form shown in Figure 2.2. The integration of the forces over the contact patch yields the net cornering force with a point of action at the centroid. The asymmetry of the force distribution within the contact patch causes a resultant force to be positioned to the rear of the centre of the contact patch by a distance known as the pneumatic trail. By SAE convention (Gillespie 1992):

> *The transverse force is taken to act about at the centre of the tyre contact. At this position the net resultant is a transverse force and an aligning moment. The magnitude of the aligning moment is equal to cornering force multiplied by the pneumatic trail*

The data on cornering force and aligning torque versus slip angle and vertical tyre load used in the computer simulations were obtained from the tyre manufacturers and from the University of Michigan Transportation Institute (taken from data on unpublished trials).

[1] Details obtained from tyre manufacturers in personal communications.

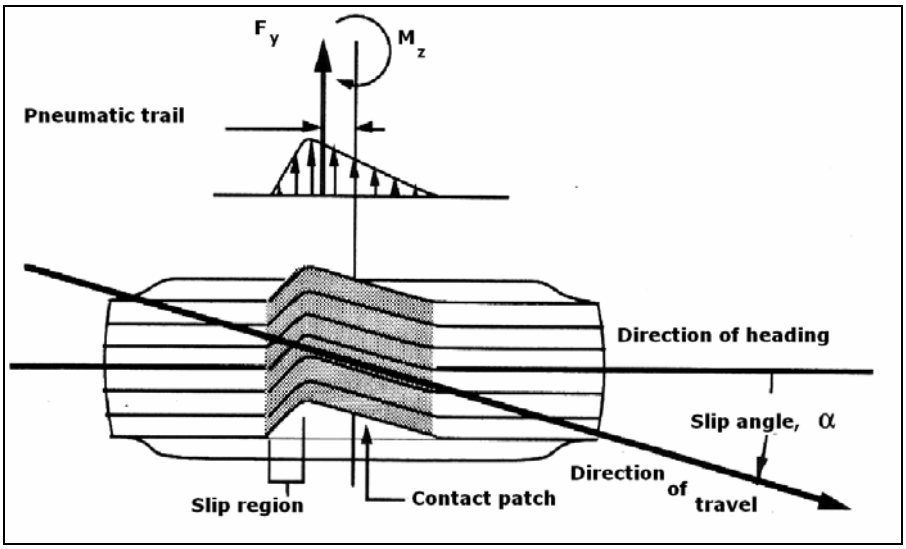

Figure 2.2 Rolling tyre deformation under a transverse force (Gillespie 1992).

On a two-axle truck with Ackerman steering[2] undergoing a low-speed turn, the tyres will roll with no slip angle and with no cornering force. But when a truck has more than one non-steering axle in an axle group, as in the tandem-drive group of a three-axle truck, it is not possible to achieve zero slip and zero cornering force on any of the tyres during the turn. Figure 2.3 shows a tandem axle group undergoing a low-speed turn. The circular arcs show the paths of the inner wheels, outer wheels, and the centre of the axle group. It can be seen that the orientation of the wheels is different from their direction of travel, i.e. they are rolling with non-zero slip angles and with non-zero cornering or scuffing forces. If the direction of travel is towards the top of the figure then the upper axle is dragged towards the centre of the curve and the lower axle is dragged away from the centre of the curve. As the axle group does not spin out of control, these forces must balance.

Assuming these axles have the same tyre configuration (the same cornering stiffness), the slip angle and cornering force on the lead non-steering axle must exceed that of the other axles in the group to achieve a cornering force balance. Thus the centre of turn must act at a location that is behind the geometric centre of the axle group. The turning behaviour of the vehicle can be modelled by replacing the axle group with a single axle known as the equivalent single axle. The model can be further simplified by eliminating the axle width and considering a wheel at the mid-point of the equivalent single axle. This is known as the bicycle model approximation.

[2] During low-speed turns over a horizontal surface, Ackerman steering proportions the steer angles on the left and right wheels of the steer axle so that their axes of rotation pass through the centre of turn. The centre of turn is located on the axis of rotation of the rear axle. Thus the tyres roll with a slip angle of zero and with zero cornering force.

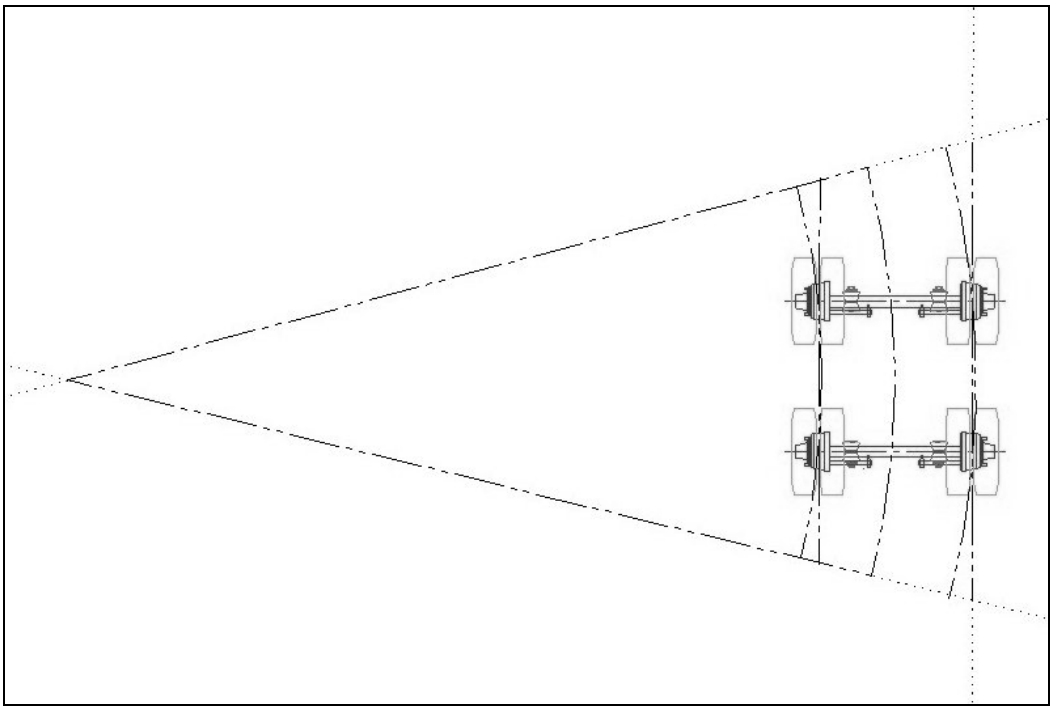

Figure 2.3 Tandem axle group executing a low-speed turn.

2.1.2 Axles and axes

The definition of the front axis of a vehicle varies with the type of vehicle. It includes the location of the lead steer axle (for powered units) and the location of the tow coupling (for simple-trailers and semi-trailers). The rear axis of a vehicle is the geometric centre of the rear axle group, assuming they have the same tyre configuration as each other. The geometric wheelbase, which is often just called the wheelbase, is the distance from the front axis to the rear axis. For simple-trailers and semi-trailers, the wheelbase is also known as the forward length. As mentioned above, the location of the equivalent single axle is behind the rear axis and so the equivalent wheelbase is slightly longer than the geometric wheelbase. Equation 2.5 (see below) shows the relationship between the geometric wheelbase and the equivalent wheelbase.

Employing the bicycle model, the slip angle and cornering force of the i^{th} axle on the j^{th} non-steering axle group belonging to the j^{th} vehicle unit can be determined. Under different cornering conditions, the cornering force can be described by:

$$f_{yij} = \begin{cases} c_\alpha(f_{zij})\,\alpha_{ij}, \text{ linear} \\ f_{yij}(f_{zij}, \alpha_{ij}), \text{ nonlinear} \\ \mu_{ys} f_{zij}, \text{ static} \\ \mu_{yk} f_{zij}, \text{ kinetic} \end{cases} \qquad \text{Equation 2.1a, b, c, d}$$

where:

$$\alpha_{ij} = \tan^{-1}\left(\frac{\delta_{ij} + \varepsilon_j}{r_j}\right) \qquad \text{Equation 2.2}$$

$$\varepsilon_{\mathrm{j}} = \frac{1}{l_{g\mathrm{j}}}\left(\frac{1}{N_{\mathrm{j}}}\sum_{\mathrm{i}=1}^{N_{\mathrm{j}}}\delta_{\mathrm{ij}}^{2}\right) \qquad \text{Equation 2.3}$$

$$r_{\mathrm{j}} = \left(r_{0}^{2} - \sum_{\mathrm{k}=1}^{\mathrm{j}}(l_{e\mathrm{k}}^{2} - h_{\mathrm{k}}^{2})\right)^{1/2} \qquad \text{Equation 2.4}$$

$$l_{e\mathrm{j}} = l_{g\mathrm{j}} + \varepsilon_{\mathrm{j}} \qquad \text{Equation 2.5}$$

$$LSO_{\mathrm{j}} = r_{0} - r_{\mathrm{j}} \qquad \text{Equation 2.6}$$

and where:

- i axle number;
- j j^{th} non-steering axle group belonging to the j^{th} vehicle unit;
- k k^{th} vehicle unit;
- f_y tyre cornering force or pavement scuffing force;
- f_z vertical force;
- α slip angle;
- c_α cornering stiffness (linear tyre model used for small slip angles only);
- μ_{ys} transverse pavement–tyre static friction coefficient;
- μ_{yk} transverse pavement–tyre kinetic or sliding friction coefficient;
- δ_{ij} displacement from the j^{th} rear axis to the i^{th} axle (positive distance forward, negative distance backward);
- ε distance from the rear axis to the equivalent single axle;
- r radius of curvature or instantaneous turn radius of the path followed by the equivalent single axle;
- r_0 reference turn radius or radius of curvature;
- l_e equivalent wheelbase: distance from the front axis to the equivalent single axle;
- l_g geometric wheelbase: distance from the front axis to the rear axis;
- h distance from the tow coupling to the corresponding equivalent single axle;
- N number of non-steering axles;
- LSO low-speed steady-state offtracking.

Equations 2.3–6 are based on those given in Fancher & Winkler (2007). Based on Equations 2.1a and b, and on Equations 2.2–5, it can be seen that a tyre's slip angle and cornering force depends on the radius of curvature of its path. This radius of curvature in turn depends on the tyre's longitudinal distance from the equivalent single axle; and on the radius of curvature of the equivalent single axle's path[3].

Equation 2.2 and Equation 2.3 show that the tyres on the lead axle in a group are furthest from the equivalent single axle compared with the other axles. Hence the slip angle and cornering force on these tyres are greater than in the other tyres in the group. On very

[3] A circle of radius r has curvature 1/r everywhere. A straight line has zero curvature everywhere.

tight turns, the tyres on the lead axle are the first to slide, in which case, the cornering force on this axle can then be described by Equations 2.1c and d. Once the lead axle starts to slide, the equivalent single axle shifts backward, increasing the equivalent wheelbase. Increasing the equivalent wheelbases increases low-speed offtracking.

Equation 2.4 is a low-speed steady-state solution and shows that the radius of curvature of the path followed by the equivalent single axle is mainly determined by the geometry of the vehicle and the turn. Substituting Equation 2.4 into Equation 2.6 gives an analytical solution for calculating the amount of low-speed steady-state offtracking.

2.1.3 Coulomb friction

For a given tyre and horizontal pavement surface, the cornering or scuffing force magnitude increases with increasing slip angle and vertical load (according to the manufacturers' data sheets (pers. comm.) and unpublished data from the University of Michigan Transport Research Institute) but is limited to a value equal to the vertical load multiplied by the coefficient of friction between the pavement–tyre interface.

The classical approximation of the force of friction between two solid surfaces in shear is known as Coulomb friction. For a horizontal pavement surface, the Coulomb friction force is proportional to the vertical load. Equation 2.1c and Equation 2.1d represent the classical friction model. The differences between these two equations are the constants of proportionality. Equation 2.1c employs the static friction coefficient and Equation 2.1d employs the kinetic friction coefficient. The force which is applied to an object that remains at rest is called the static friction force. The static friction force acts in the opposite direction to the applied force. As the applied force increases, the static friction force reaches a limiting value, and the object 'breaks away' and is set in motion. The friction force that then opposes the motion is called the kinetic or sliding friction force. The static friction force is greater than the kinetic friction force and limits the cornering force by:

$$-\mu_{ys} f_z \leq f_y \leq \mu_{ys} f_z \qquad \text{Equation 2.7}$$

2.2 Load transfer

2.2.1 Basic definitions

Load transfer is the redistribution of the total vehicle weight between the individual tyres during acceleration. Load transfer from body forces acting on the sprung mass occur when braking and when accelerating forward (longitudinal acceleration), when cornering (centripetal acceleration), and when in the presence of road cross-slope (gravitational acceleration). Load transfers from surface forces include directional control forces applied at the tow coupling, at the roll centre of the suspension, and at the pavement–tyre interface. Load transfer is necessary to maintain a moment balance.

Tyre forces are transmitted from the unsprung mass (tyre and axle masses) to the sprung mass (vehicle tare and payload masses) and vice versa through the suspension. The point at which these forces are transmitted through the suspension is characterised by the roll centre. The SAE (Gillepsie 1992) defines the roll centre as:

> *The point in the transverse vertical plane through any pair of wheel centers at which lateral forces may be applied to the sprung mass without producing suspension roll.*

In general, a heavy vehicle's sprung mass centre of gravity (CG) is located some distance above the roll centre of the suspension, and the roll centre is in turn located some distance above the ground plane. Most heavy vehicles are constructed from a series of solid axles[4] for a number of reasons including the simplicity of design, strength, durability, and cost. The roll centre of a suspension with a solid axle can be assumed to be located at a fixed position beneath the sprung mass.

Lateral load transfer is defined as the difference between the vertical load on one side of an axle and that on the other side. The amount of vertical load on a particular tyre group can therefore exceed the static vertical load. Assuming that the roll centre is at a fixed position beneath the sprung mass and ignoring the unsprung mass for simplicity, the lateral load transfer for a solid single-axle simple-trailer undergoing a steady-state left turn over a horizontal surface is given by:

$$f_{zr} - f_{zl} = \frac{2}{t_t}\left(h_{rc}\left(f_{yb} + f_{ys}\right) + k_c\varphi\left(h_{rc}, f_{yb}, f_{ys}\right)\right) \qquad \text{Equation 2.8}$$

where:

- f_{zr} vertical force on the right tyre group;
- f_{zl} vertical force on the left tyre group;
- f_{yb} lateral body force acting on the sprung mass;
- f_{ys} lateral surface force applied to the sprung mass;
- t_t tyre track width;
- h_{rc} roll centre height above the ground plane;
- k_c composite roll stiffness;
- Φ body roll angle relative to the vertical axis.

[4] A solid axle has wheels mounted at either end of a rigid beam.

Equation 2.8 is based on an equation given in Gillespie (1992) and describes the lateral load transfer affects from both the lateral body and surface forces. Note that the first and second components on the right-hand side of Equation 2.8 are dependent, i.e. they each depend on the roll centre location and on the lateral forces defined. The equation indicates that increasing the tyre track width reduces the amount of lateral load transfer. Lateral load transfer, in general, arises from two mechanisms (Gillispie 1992):

- the elevated roll centre above the ground plane, and
- body roll.

The elevated roll centre above the ground plane arises from the lateral force imposed on the axle. It is independent of body roll and the longitudinal roll moment distribution. Consider a tandem axle group undergoing a low-speed steady-state turn over a horizontal pavement where the lateral body force can be ignored and thus set equal to zero. The tyre-spread across the axle group induces transverse shear forces that act at the pavement–tyre interface. Since the roll centre of the suspension is some distance above the ground plane, a roll moment is induced at the roll centre. To maintain a moment balance about the roll centre, load must be transferred laterally from one side of an axle to the other. This lateral load transfer increases with increasing roll centre height and with axle group spread.

The effect of body roll is to shift the CG of the sprung mass centre outboard of the roll centre location. It is directly dependent on the roll moment distribution. Consider a tandem axle group undergoing a low-speed steady-state turn over a horizontal pavement where the lateral body force can be ignored and thus set equal to zero. Lateral load transfer caused by body roll can be induced by tow coupling forces applied at a vertical distance offset from the roll centre, but this effect is only significant for large articulation angles. No lateral load transfer caused by body roll will occur if the tow coupling is at the same height as the roll centre of the suspension, i.e. the lateral load transfer component caused by body roll is equal to zero in this instance.

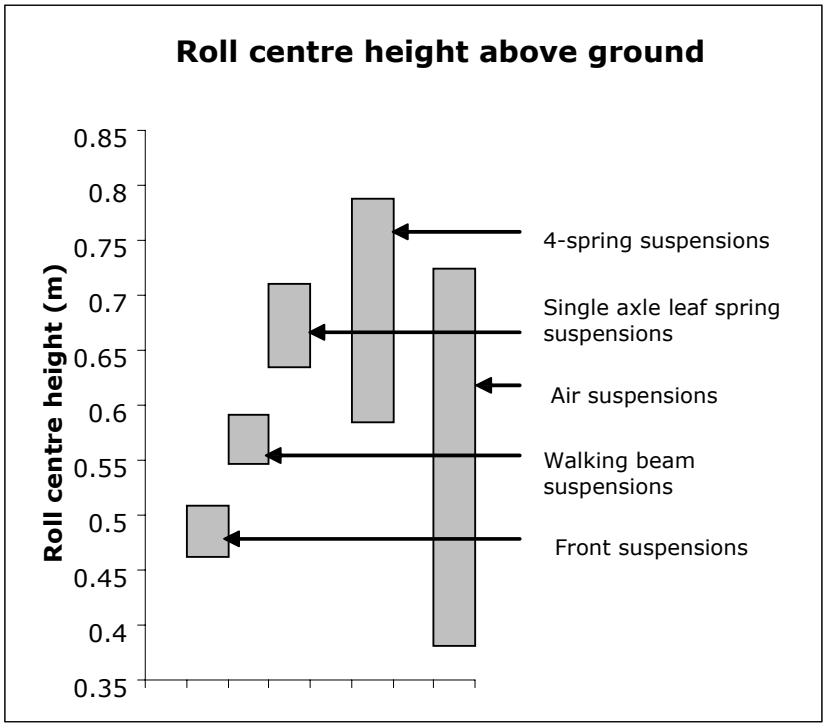

Figure 2.4 Roll centre heights for different suspensions (UMTRI 2000).

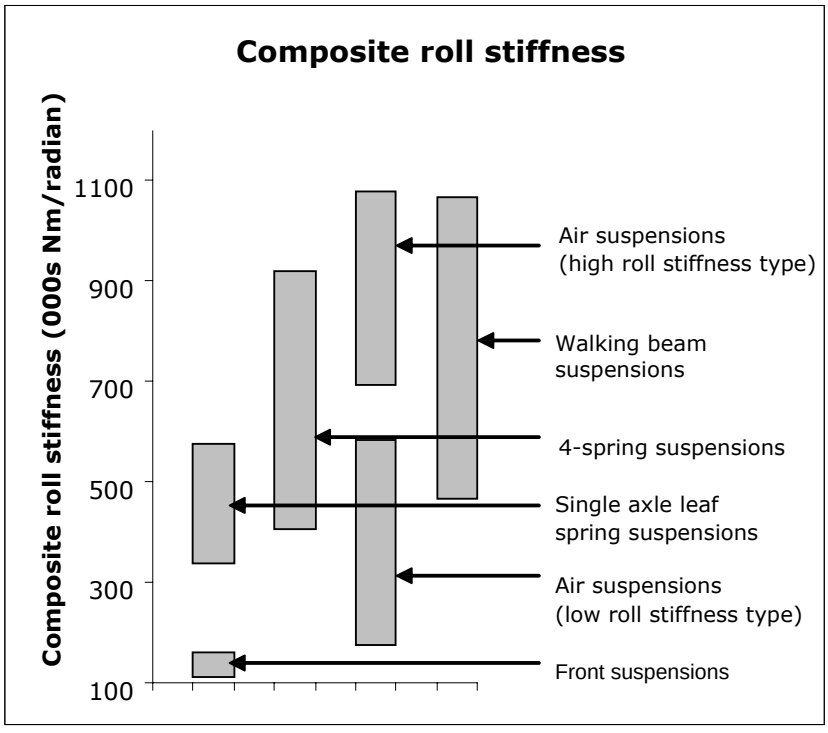

Figure 2.5 Composite roll stiffness for different suspensions (UMTRI 2000).

Figure 2.4 gives the roll centre heights and Figure 2.5 gives the composite roll stiffness for different suspensions. Note that air suspensions cover the greatest range of roll centre heights and roll stiffness. Suspensions with low roll centres and high composite roll stiffness produce low amounts of lateral load transfer.

2.2.2 Coupling types

The three main coupling types used to connect individual vehicle units in combination vehicles are fifth wheel, turntable, and tow-eye couplings. The main difference between these coupling types is the number of rotational degrees of freedom they permit. The suspension systems for vehicle units that are roll coupled contribute to the overall roll moment distribution between these units. Lateral load transfer caused by body roll is directly dependent on this roll moment distribution.

A fifth wheel coupling is used for semi-trailer connections and is often referred to as a B-coupling. It consists of a kingpin that interlocks with a U-shaped skid plate. The coupling allows a semi-trailer to yaw with respect to the towing vehicle. A conventional single oscillating fifth wheel coupling allows some moments about the roll and pitch axis to be transmitted between these two vehicles. The magnitude of these components depends on the articulation between these vehicles, with the roll and pitch components being proportional to the cosine and sine of the articulation angle, respectively. Thus at zero articulation angle, only the roll moment is transmitted.

A turntable coupling consists of a ball race system that connects a semi-trailer to a dolly to form a full-trailer. A turntable allows only yaw motion between these vehicles. Both roll and pitch moments are transmitted between these units. A pitch hinge connects the dolly's bogey to the dolly's drawbar. This prevents pitch moments generated at the dolly from applying vertical loads at the tow-eye coupling. The dolly's turntable, bogey, and drawbar assembly is often referred to as an A-coupling.

A tow-eye coupling consists of a towing eye that interconnects with a pin or a hook, and is functionally equivalent to the ball and cup arrangement used on light trailers. The coupling provides no restraints on rotational motion. It connects two vehicle units together that are free to yaw, roll, and pitch with respect to one another. No lateral load transfer caused by body roll occurs between tow-eye coupled units.

2.2.3 Load transfer v. rollover performance

Rollover stability, which is characterised in terms of the Static Roll Threshold (SRT), and lateral load transfer are directly related. When wheel lift-off occurs at the onset of a rollover, the load has been transferred completely from one side of an axle to the other side.

Fully laden heavy vehicles typically have relatively high sprung mass values and sprung mass CG heights. When heavy vehicles undertake high-speed turns, the lateral body forces are significant. In this situation, the lateral load transfer component caused by body roll is usually the more critical of the two lateral load transfer mechanisms. The effect of body roll is to shift the CG of the sprung mass centre towards the outside of the turn, unloading the inside wheels and increasing the load on the outside wheels. The amount of body roll can be reduced by increasing the composite roll stiffness. Lateral load transfer can be reduced by increasing the tyre track widths. In both cases, an improved SRT will result.

2.3 Low-speed v. high-speed directional performance

An analytical solution of a linear two-axle full-trailer model, given in Fancher & Winkler (2007) shows how longer wheelbases and higher cornering stiffnesses can reduce rearward amplification. The analysis deduced that longer vehicles have more damping of yaw motions than comparable vehicles with shorter wheelbases and that this damping increases with the square of the wheelbase. Fancher & Winkler also found that increasing the cornering stiffness increases damping in yaw rate and in lateral velocity. Increasing cornering stiffness is also known to reduce high-speed steady-state offtracking.

Improved low-speed directional performance can be characterised by a vehicle having less low-speed offtracking. Improved high-speed directional performance can be characterised by a vehicle having less high-speed steady-state offtracking and more yaw damping. A vehicle having more yaw damping is typically associated with it having less rearward amplification and less high-speed transient offtracking. A rule of thumb given by Fancher & Winkler was:

> *…what one does to improve low speed performance is likely to degrade high speed performance and vice versa.*

For the same overall vehicle length, combination vehicles with more articulation joints and shorter wheelbase units generally have good low-speed directional performance, but also have poor high-speed directional performance than combination vehicles with fewer articulation joints and longer wheelbase units.

Increasing the number of non-steering axles within a group usually leads to an overall increase in axle group spread and cornering stiffness. These changes result in higher scuffing forces but can improve high-speed directional performance. For similar reasons, a non-steering axle group has a higher overall cornering stiffness, which will generate more scuffing force, but it will have better high-speed directional performance than a comparable self-steering axle group.

2.4 Self-steering axles

The purpose of self-steering or castoring axles is to reduce the transverse pavement scuffing and tyre scrubbing forces generated by the tyres of multi-axle groups during low-speed turns (Latto & Baas 2002). Self-steering axles are steered passively about the kingpin by the applied cornering force at the pavement–tyre interface at a trailing distance behind the kingpin.

Many self-steering axles have mechanisms that provide a steering stabilisation or centring force. Undulating pressure bearings can be used to provide a weight dependent centring force. In some cases, steel and air springs are used to provide a centring force, the latter requiring an extraneous power source (Latto & Baas 2002). Air springs have the potential to provide a variable centring force by altering the airbag pressure. Locking mechanisms are used to provide very large centring forces and are often used when the vehicle is reversing, but can also be used at higher speeds. The foremost self-steering axle on quad-axle groups in New Zealand may be locked in the straight-ahead position at a speed of 30km/h or more (Land Transport New Zealand (LTNZ) 2007). Having a weight and speed dependent centring force can provide a mechanism for improved low-speed and high-speed directional performance. All axle groups on heavy vehicles except for front twin-steer axle groups on powered units must be load sharing (Land Transport Safety Authority (LTSA) 2002).

The self-steering axle characteristics used in the analysis are given in Table 2.1 and Figure 2.6. The figure shows the steering torque as a function of steer angle. The steering torque is equal in magnitude to the applied centring force multiplied by the trailing distance behind the kingpin. The axles have steer angle limits of 15°, which is the minimum required by the Vehicle Dimensions and Mass (VDM) Rule. At this steer angle, the steering torque increases to a very large value which effectively simulates the self-steering axles hitting their stops.

Table 2.1 Self-steering axle system parameters.

Parameter	Unit	Value
Primary stiffness	Nm/rad	2 589 422
Coulomb friction	Nm	1235
Mechanical trail	mm	151

A rigid truck without a heavy tow coupling, or a semi-trailer not belonging to an A or B-train may have steering axles in the rear axle group so long as no more than half of these axles steer at any time (LTSA 2002). This means that rear-mounted tandem or tridem axle groups on conforming vehicles may not have more than one self-steering axle. Quad-axle groups, which are only permitted on semi-trailers not belonging to an A or B-train, are required to have two self-steering axles (LTSA 2002). Although these can be either the first and last axles, or the two trailing axles, the requirements of the bridge formula and other dimensional constraints mean that on quad-axle groups, the self-steering axles are almost always the two trailing axles. For similar reasons, the self-steering axle on rear-mounted tandem and tridem axle groups on conforming vehicles is almost always the rear axle.

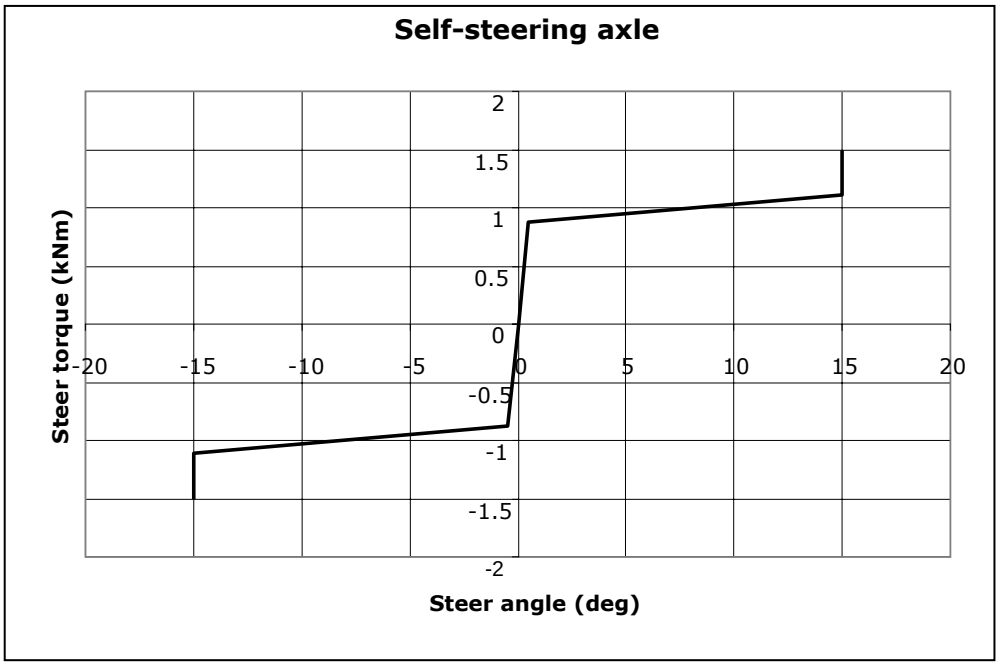

Figure 2.6 Steer torque v. steer angle for the self-steering axle.

2.5 Simulation software

The computer simulation software used in this study was the Constant Velocity Yaw-Roll Multi-Body simulation package from the University of Michigan Transportation Institute. The software has been used extensively in New Zealand and internationally to undertake performance assessments of heavy vehicles. It has been experimentally validated both internationally and in New Zealand. In this report, this software is referred to as the Yaw-Roll simulation software. Some simplifying mathematical assumptions have been employed by this software (Gillespie 1982):

- Constant velocity means that no tractive or braking forces are incorporated in the model.
- The vehicle models traverse a horizontal pavement with uniform friction characteristics.
- A single peak friction coefficient defines the friction model. This implies that the static friction coefficient is equal to the kinetic friction coefficient.
- Camber thrust is not incorporated in the model.
- The small angle approximation holds for the pitch motion of the sprung mass and for the relative roll angle between the sprung mass and unsprung mass.
- The relative roll motion between the sprung mass and unsprung mass takes place about the roll centre, which is at a fixed distance beneath the sprung mass.
- Forces acting on each axle are treated independently; therefore, no inter-axle load transfer effects are incorporated in the model. The axles are modelled as solid axles.

3. Field trial

3.1 Location

The field trial was undertaken to assess the level of scuffing force required to cause visible wear on chipseal pavements and to provide some validation of the Yaw-Roll simulation software. The physical testing was done on a dry section of road that was formerly part of State Highway 1 but is now a local access road. This location was at the southern end of Ohinewai South Road which is about 6 km north of Huntly in the central North Island (marked with a star on the map in Figure 3.1). The pavement construction was a matured unbound granular structure with chipseal surfacing. The range of pavement surface temperatures over the course of the trial was 19–21^{o}C.

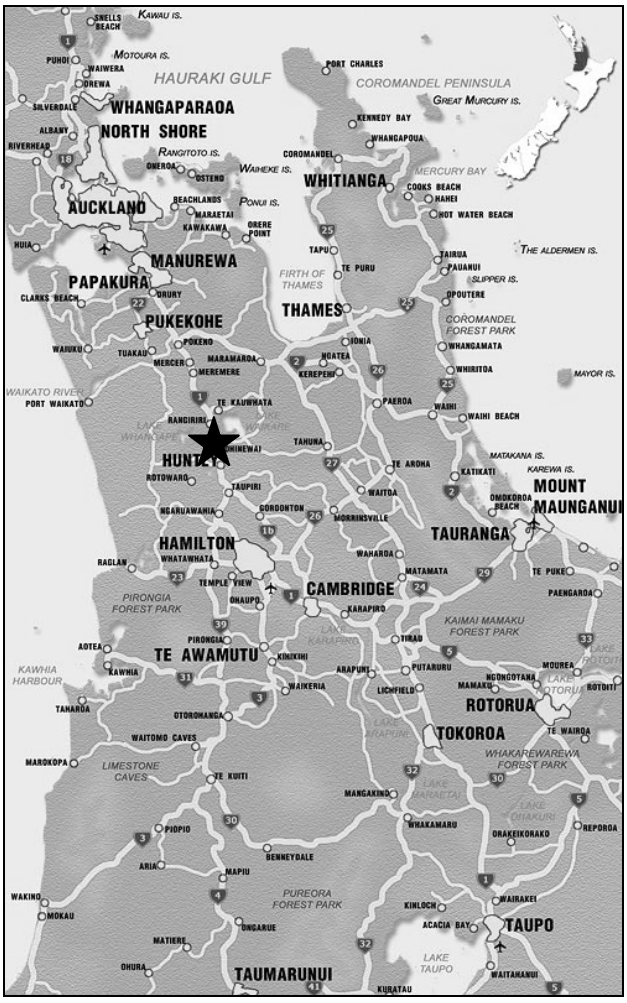

Figure 3.1 Map showing the location of the field trial.

3.2 Experimental methodology

For this test, a three-axle full-trailer with a single-axle dolly was jack-knifed. The vehicle had single-leaf steel spring suspension with dual 255/70R22.5 tyres inflated to 100 psi. The drawbar was towed at a constant crawl speed perpendicular to the trailer's alignment, and the towing force was measured. The scuffing forces generated by the tyres of the trailer's tandem axle group represent an extreme case of scuffing forces (kinetic or sliding) where very large slip angles are induced. The mechanism responsible for these extreme cases of scrubbing forces differs from that generated by a rolling tyre where much smaller slip angles apply (non-sliding case). This manoeuvre was repeated for three tandem axle group loads of approximately 7 tonnes, 10 tonnes, and 13 tonnes. The tare weight of the tandem axle group was 4100 kg and the load consisted of concrete blocks, each weighing 940 kg on average. A hydraulic hoist (Hiab) attached to the rear of the truck was used to lift the concrete blocks in and out of the trailer. Figure 3.2 shows the trailer jack-knifed into position ready to be pulled forward in the thirteen tonne experiment.

The towing force was measured using a calibrated load cell chained between the towing eye of the drawbar and the pin coupling of the truck (tow-eye coupling). The load cell in this arrangement measured tensile forces only. The towing force data sampled at 50 Hz was passed through a zero-phase low-pass digital Butterworth filter and then zeroed with respect to the global minimum for that run (see Figure 3.3). The eighth order Butterworth filter had a cutoff frequency of 4 Hz.

Figure 3.2 The test vehicle jack-knifed into position ready to be driven forward and the towing force measured in the thirteen tonne experiment.

The average kinetic scuffing force generated by the tyres of the tandem axle group was back-calculated from the peak kinetic towing force by employing the bicycle model, defined in terms of the trailer's dimensions and the static vertical loads per tyre group. The bicycle model eliminates the axle width by considering a wheel at the mid-point of the axle. Moments were balanced about the location of the equivalent single axle of the tandem axle group and the following relationship was derived:

$$f_{yt} = \frac{2s}{l_e}\mu_{yk}f_{z0} + f_{yd} \qquad \text{Equation 3.1}$$

where:

$$f_{ya} = \mu_{yk}f_{z0} \qquad \text{Equation 3.2}$$

and where:

- f_{yt} peak kinetic towing force (vector);
- f_{z0} static vertical load per tyre group (vector);
- f_{ya} average kinetic scuffing force per tyre group (vector);
- f_{yd} drag force of dolly;
- l_e equivalent wheelbase of 6.15 m;
- s tandem axle group spread of 1.35 m;
- μ_{yk} transverse coefficient of kinetic friction.

Equation 3.1 was used to calculate both the dolly's drag force and the transverse coefficient of kinetic friction at the pavement–tyre interface. The dolly's drag force was calculated by fitting a line to the peak kinetic towing force versus static vertical load data using linear least-squared regression analysis and retrieving the y-intercept. The slope of this line was used to calculate the transverse coefficient of kinetic friction. This is shown in Figure 3.4.

3.3 Simulation methodology

A similarly configured computer model of a tandem simple-trailer was used to simulate the forces observed in the field trial so we could verify the results. The model's tare weight and load mass was centred above the rear axis of the tandem axle group so that no static vertical load was placed on the coupling. A tow-eye coupling was used to eliminate any rotational coupling between the truck and trailer. This is functionally equivalent to the actual full-trailer used in the field trial, where the single-axle dolly (with pitch hinge) had an articulation angle of 90^{o} with respect to the trailer's alignment. The relevant tyre, suspension, and trailer data used in this analysis are given in Appendix A.

The Yaw-Roll simulation software initialises the vehicle model in a straight line and not in the jack-knifed position as in the field trial. To reproduce the kinetic scuffing forces observed in the field trial, the tow-eye coupling of the trailer model would ideally undertake a steady-state cornering manoeuvre with a turn radius equal to the equivalent wheelbase of the trailer of 6.15 m while travelling at 1.8 km/h. During the turn, however, the vehicle model could not reach the desired stead-state cornering condition and so the simulated scuffing forces are slightly underestimated compared with those calculated in the field trial.

3.4 Results

Figure 3.3 shows the raw and filtered towing force data for the seven tonne gross tandem axle group mass experiment. Three characteristic towing force extrema are located in this example at 10.05 seconds (s), 10.15 s, and 14.5 s into the manoeuvre. The local maximum at located 10.05 s and the local minimum located at 10.15 s into the manoeuvre are representative of the peak static friction force and the peak kinetic friction force experienced at the pavement–tyre interface, respectively. Between 10.15 s and 14.5 s, the towing force begins to increase but this increase in towing force is from accelerating the rearmost trailer unit (excluding the dolly). The global maximum, located 14.5 s into the manoeuvre, is the point where the driver engages the clutch, allowing the vehicle combination to slow to a stop.

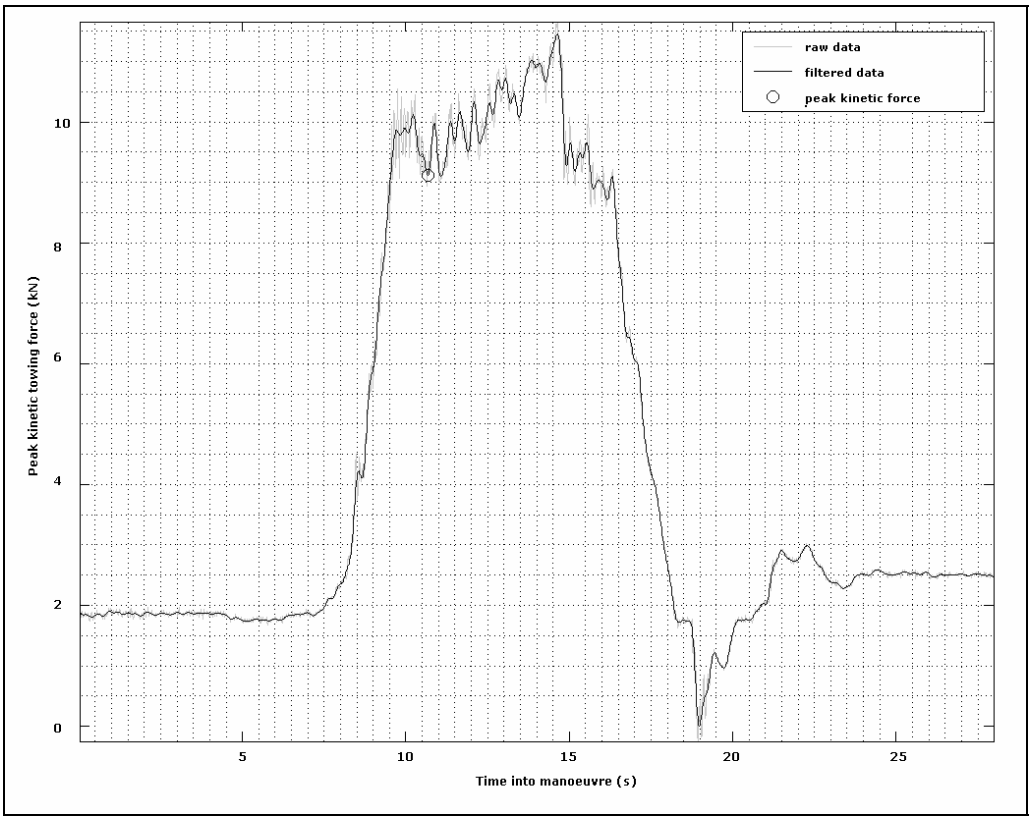

Figure 3.3 Extraction of the peak kinetic towing force for the seven tonne gross tandem axle group mass experiment.

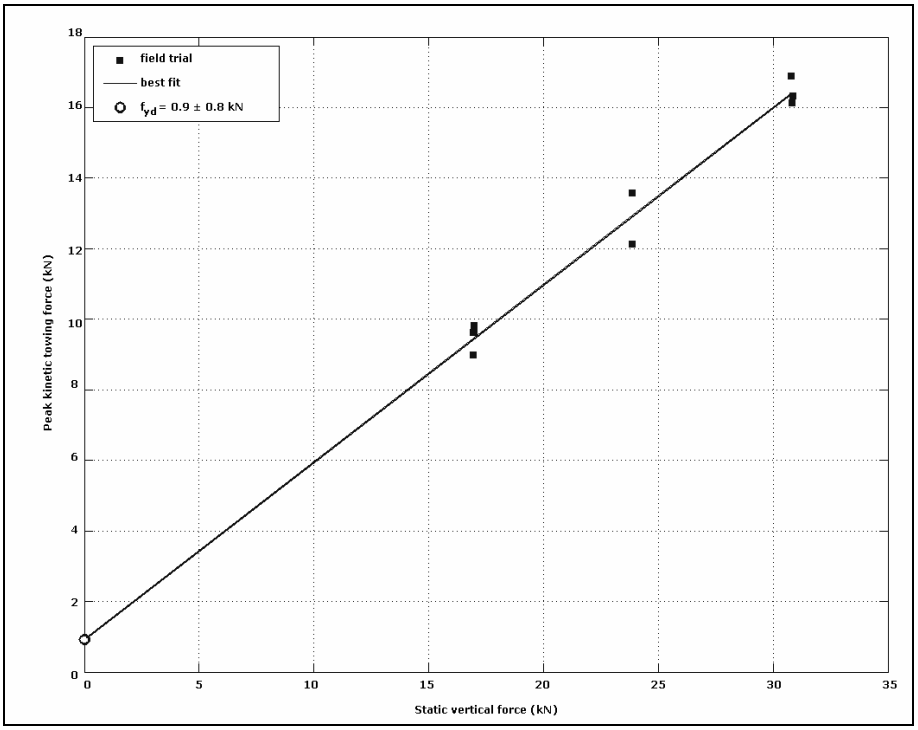

Figure 3.4 Line of best fit for the peak kinetic towing force v. static vertical force.

Notes to Figure 3.4:
μ_{yk}(transverse coefficient of kinetic friction) = 1.15±0.03
fyd = drag force of dolly

Figure 3.4 shows the line of best fit of the peak kinetic towing force versus the static vertical load. The drag force of 0.9±0.8 kN accounts for the rolling resistance of the single axle dolly, which had a gross axle weight of 1900 kg. The corresponding rolling resistance coefficient of 0.05±0.04 is in line with typical values for truck tyres on medium to hard surfaces of 0.06 (Gillespie 1992). The calculated transverse coefficient of kinetic friction between the pavement–tyre interface was 1.15±0.03. The drag force, rolling resistance, and coefficient of friction values are calculated with 68.27% confidence intervals (assuming normally distributed independent samples). No data were available on the transverse coefficient of kinetic friction between dry chipseal pavements and heavy trailer tyres. However, this value does seem reasonable, given that both the chipseal and tyres were in very good condition.

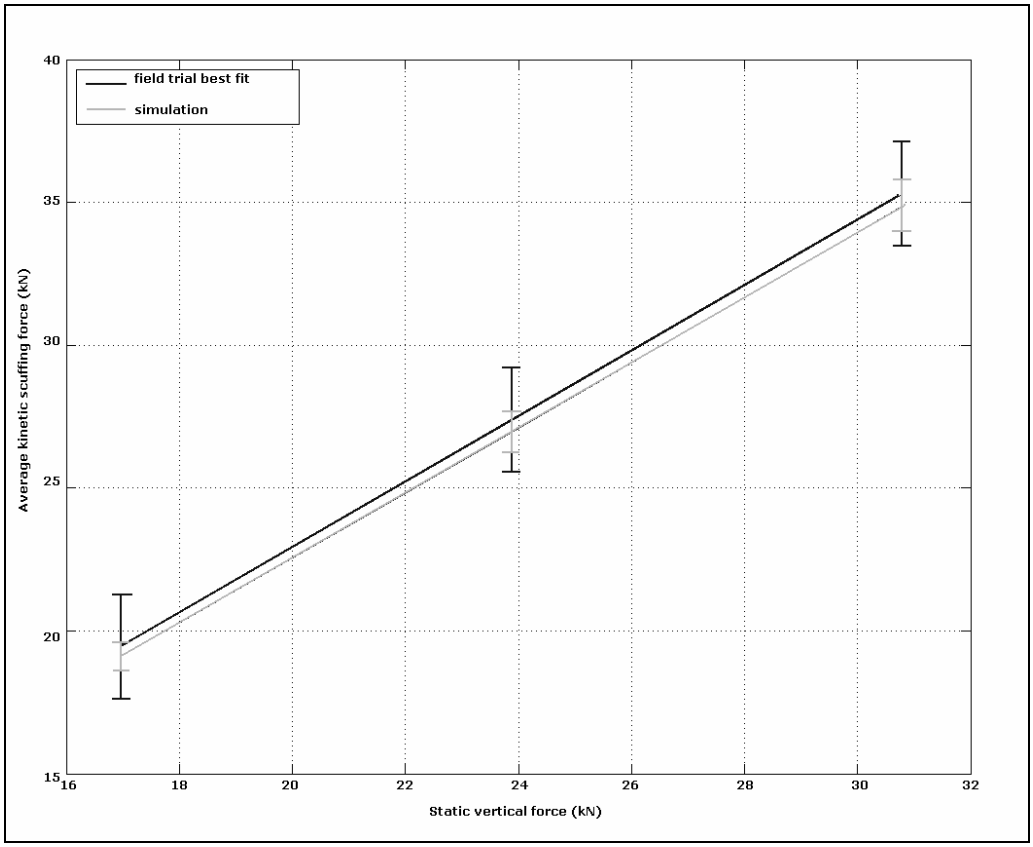

Figure 3.5 Average kinetic scuffing force v. static vertical force comparing the field trial and simulation data.

Figure 3.5 shows the average kinetic scuffing force versus the static vertical load, comparing the field trial and simulation data. The field trial and simulation software results are in good agreement with each other, and they verify that the average kinetic scuffing force is proportional to the static vertical load. The error bands in the field trial best fit data represent the uncertainty in the dolly's drag force calculation, and the error bands in the simulation data represent the uncertainty in the coefficient of kinetic friction calculation. Note that the Yaw-Roll software was not designed for severe cornering manoeuvres, and so the simulated scuffing force data are slight underestimates compared with those calculated in the field trial.

Figure 3.6 Pavement scuffing damage from the seven tonne experiment.

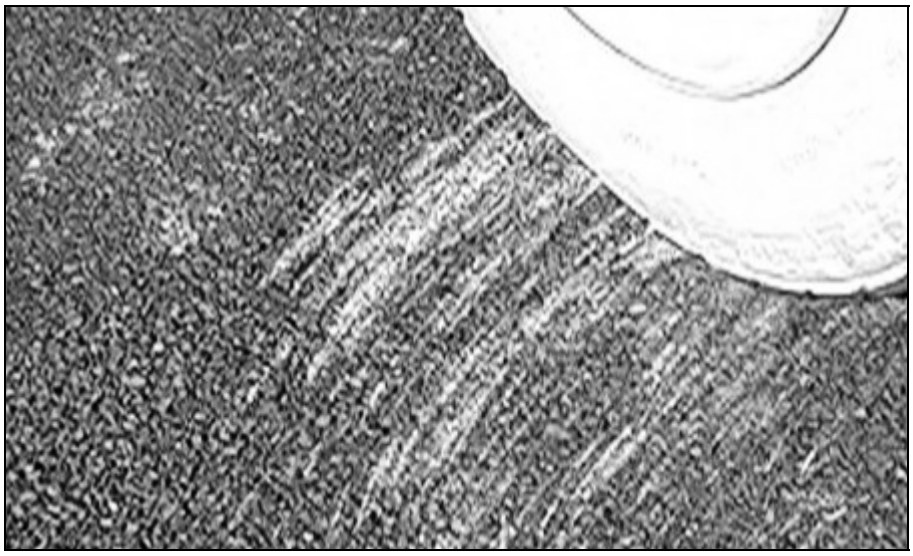

Figure 3.7 Pavement scuffing damage from the thirteen tonne experiment.

Figures 3.6 and 3.7 show the pavement scuffing damage from the seven tonne and thirteen tonne experiments, respectively. Minor visible abrasion of the chipseal surface was observed in the field trial even at the lowest gross tandem axle group load of seven tonnes. Small fragments approximately 1 mm in diameter were broken off the exposed corners of the chip. Based on the computer simulation data, this damage resulted from a peak scuffing force of at least 33.2 kN. The corresponding vertical load of 28.9 kN is 70% above the static vertical load of 17.0 kN. Note that the peak scuffing force of 33.2 kN is equal to 1.15 multiplied by the vertical load of 28.9 kN. More severe abrasion of the chipseal surface was observed in the 13 tonne experiment – compare Figures 3.6 and 3.7.

3.5 Discussion

The field trial and simulation software results are in good agreement with each other, and they verify that scuffing force is proportional to static vertical load. Minor visible abrasion of the chipseal surface was observed in the field trial at the lowest gross tandem axle group load (a little under 7 tonnes), where small fragments approximately 1 mm in diameter were broken off the exposed corners of the chip. Based on the computer simulation, this damage resulted from a peak scuffing force of at least 33.2 kN. Note that in general, the pavement wear resulting from scuffing forces will depend on many factors including:

- the overall pavement design (seal, base, subgrade);
- the condition of the pavement (e.g. age, rehabilitation or replacement); and
- various environmental factors (e.g. temperature, water, ice).

4. Computer simulations

4.1 Model parameters

Computer simulations were undertaken to see how scuffing forces are influenced by changes in turn geometry and vehicle parameters, namely:

- angle of turn,
- turn radius,
- wheelbase,
- number of non-steering and self-steering axles,
- axle group spread,
- axle weight,
- tyre size, and
- dual tyres versus wide-single tyres,

Simple-trailer computer models were used to assess the effects of axle load, axle group spread, wheelbase, and turn geometry on scuffing forces. Computer models for typical heavy vehicles, axles, and tyre configurations currently used in New Zealand were used to simulate various low-speed turns, and the relative impact of scuffing forces for the different vehicles are identified. The vehicle models used steel spring suspension. The tyre and suspension data used in this analysis are given in Appendix A.

The couplings of the simple-trailer models and the lead steer axle centres of the vehicle models were made to follow circular paths with straight entry and exit tangents at a constant speed of 1.8 km/h. A turn radius[5] of 13.75 m was used to construct the simple-trailer and vehicle performance maps. The simple-trailer and vehicle computer models are configured with dual 11R22.5 tyres on the drive and trailer axles, and with single 11R22.5 tyres on the steer axles. In addition to these performance maps, four reference vehicles were used to compare the scuffing forces generated by dual 11R22.5 tyres and dual 245/70R19.5 tyres, and by 385/65R22.5 wide-single trailer tyres. To compare the scuffing forces generated by the different tyre configurations, the reference vehicles undertook a turn radius of 18.75 m. The larger 18.75 m radius of turn was needed since tyre data for the 245/70R19.5 and 385/65R22.5 tyres were only available for slip angles of up to 6^{o}, whereas tyre data for the 11R22.5 tyres were available for slip angles of up to 12^{o}. Larger radius turns induce smaller angles of slip. Note that the mechanism responsible for the scuffing forces in this section, which are generated by rolling tyres (the non-sliding case), differs from that of the field trial where much larger slip angles

[5] The turn radius of 13.75 m corresponds to the general minimum radius (i.e. 15 m less half the nominal heavy vehicle width of 2.5 m) for the design single-unit and semi-trailer turning paths specified in the *AUSTROADS Guide to Traffic Engineering Practice – Intersections at Grade* (AUSTROADS 1995).

apply (kinetic or sliding case). Unless otherwise stated, the peak coefficient of friction used in the computer simulations was 1.0.

4.2 Simulation methodology

4.2.1 Scuffing force and vertical load

For a given computer simulation, the peak scuffing force was found along with the tyre group's slip angle, vertical load, and axle number. In addition, the amount of lateral load transfer expressed as a percentage of the tyre group's static vertical load was calculated for the different vehicles by the following equation:

$$\Delta_{zp} = 100\% \left(\frac{f_{zp}}{f_{z0}} - 1 \right) \qquad \text{Equation 4.1}$$

where:

- Δ_{zp} lateral load transfer expressed as a percentage of the static vertical force;
- f_{zp} vertical force on the tyre group;
- f_{z0} static vertical force on tyre group.

Four reference vehicles were used to compare the peak scuffing forces generated by dual 245/70R19.5 tyres and by 385/65R22.5 wide-single tyres relative to dual 11R22.5 tyres. The reference vehicles are described in Table 4.3. The percentage change in peak scuffing force of a particular tyre configuration relative to dual 11R22.5 tyres is given by:

$$\Delta_{ypt} = 100\% \left(\frac{f_{ypt}}{f_{yp0}} - 1 \right) \qquad \text{Equation 4.2}$$

where:

- Δ_{zp} percentage change in peak scuffing force of tyre configuration *t* relative to dual 11R22.5 tyres;
- f_{yp0} peak scuffing force of dual 11R22.5 tyres;
- f_{ypt} peak scuffing force of tyre configuration *t;*
- *t* tyre configuration: dual 11R22.5, dual 245/70R19.5, or wide-single 385/65R22.5 tyres.

The changes in tyre size and configuration resulted in changes in vertical stiffness, unsprung and sprung mass CG heights, roll centre heights, and tyre track widths – see Appendix A. The tyre track width depends on the width of the tyre and on the tyre configuration (single or dual tyre group). The overall tyre track width is conserved. The overall tyre track width is measured from the outer tyre walls excluding the lower bulge.

The simulation outputs are sampled at 5 Hz and the results passed through a zero-phase low-pass digital Butterworth filter. The eighth order digital Butterworth filter had a cutoff frequency of 0.25 Hz.

4.2.2 Simple-trailer performance maps

The tandem and tridem simple-trailers are modelled with different weights and dimensions undergoing various low-speed turns. To eliminate the offtracking effects of the truck on the trailer, the coupling was made to follow the prescribed turning paths. The sprung mass of the trailer was centred directly above the rear axis of the axle group so that no static vertical load was applied to the coupling. A tow-eye coupling was used to eliminate any rotational coupling between the truck and trailer. The tow coupling height was set equal to the roll centre height of the suspension so that no lateral load transfer from body roll was induced.

4.2.3 Vehicle performance maps

Vehicle performance maps were constructed for a range of vehicles undergoing various low-speed turns. The vehicle models in this study comply with the VDM rule. The maximum vehicle width permitted by the VDM Rule is 2.5 m. The maximum overall length permitted by the VDM Rule is 18 m for tractor semi-trailers; 20 m for B-trains, and truck and full-trailers. The maximum Gross Vehicle Mass (GVM) for these vehicles is 44 tonnes. For the given axle group spreads, the axle group masses on the five-axle and six-axle tractor semi-trailers and single-unit truck reflect the maximum axle group mass limits permitted by the VDM Rule. For the eight-axle tractor semi-trailers, B-trains, and truck and full-trailer combinations, the GVM requirement of 44 tonnes was the limiting factor rather than the axle group mass limits. For vehicles where the GVM of 44 tonnes was the limiting factor, the axle group masses reflect those typically encountered in the transport industry. The axle group spreads for the tandem, tridem, and quad-axle groups are 1.35 m, 2.70 m, and 4.00 m, respectively. The relevant vehicle and suspension parameters used in the simulations are given in Appendix A.

To represent the vehicle configurations in a descriptive and compact form, a shorthand code called the Tyre-Axle-Coupling (TAC) sequence has been developed. The TAC sequence is a string of case-sensitive context-dependent characters used to encode the type of couplings, axles, and tyre configurations used throughout a vehicle's configuration. Tables 4.1–3 describe the set of characters used in a TAC sequence.

Table 4.1 Description of axle types and tyre configurations with the designated TAC characters.

Axle type	Tyre configuration	
	Single	Dual
Actively steered axle	a	A
Passively steered axle (self-steering axle)	p	P
Non-steering drive axle	d	D
Non-steering fixed axle	f	F

Table 4.2 Description of coupling types with the designated TAC character.

Coupling type	Coupling
Chassis	-
Fifth wheel, kingpin, and semi-trailer chassis	^
Tow-eye, drawbar, and turntable (dolly)	_

For example, the TAC sequence aa-DD^pffp denotes a twin-steer tandem-drive tractor in combination with quad-axle semi-trailer with front and rear-mounted self-steering axles. The tyres on the drive axles are in dual configuration and the remaining axles are configured with single tyres. The TAC sequence a-DD_F-FF denotes a three-axle tandem-drive truck in combination with a three-axle full-trailer with a single-axle dolly. All tyres on the truck and full-trailer combination are in dual configuration except for the steer tyres, which are configured as singles. In this study, all tyres on the powered units are 11R22.5 tyres and all single trailer tyres are wide-single tyres since this is the common tyre configuration on New Zealand's heavy vehicles. A description of the vehicle models studied and their TAC sequences are shown in Table 4.3. The reference vehicles in Table 4.3 include the dual and wide-single trailer tyre variants.

Table 4.3 TAC sequence and vehicle description.

TAC sequence	Vehicle description
a-DD	three-axle truck
a-DD^FF	five-axle tractor semi-trailer (tandem-semi)
a-DD^FFF & a-DD^fff	six-axle tractor semi-trailer (tridem-semi)*
a-DD^FFF^FF & a-DD^fff^ff	eight-axle B-train*
a-DD^FFF^FFF	nine-axle B-train
a-DD^FFP	six-axle tractor semi-trailer (tridem-semi) with a single rear-mounted self-steering axle
a-DD^FF^FF	seven-axle B-train
a-DD_F-FF	six-axle truck and full-trailer
a-DD_FF-FF	seven-axle truck and full-trailer
aa-DD^FFPP & aa-DD^ffpp	eight-axle tractor semi-trailer (quad-semi) with twin rear-mounted self-steering axles*
aa-DD^PFFP	eight-axle tractor semi-trailer (quad-semi) with front and rear-mounted self-steering axles
aa-DD_FF-FF & aa-DD_ff-ff	eight-axle truck and full-trailer*

***** Reference vehicles

Note that A-trains are limited to a GVM of 39 tonnes since they exhibit unfavourable dynamic stability characteristics. As a result, A-trains have become less popular than other vehicles, which are permitted to operate at a maximum GVM of 44 tonnes. Currently, A-trains make up only a very small proportion of the heavy vehicle fleet in New Zealand and are not considered in this study.

5. Results

5.1 Abbreviations

In the performance maps and tables in this chapter, the following abbreviations have been used:

- l_g geometric wheelbase: distance from the front axis to the rear axis,
- r_0 reference turn radius,
- Θ turn angle,
- μ_p peak coefficient of friction at the pavement–tyre interface,
- f_{z0} static vertical force,
- s axle group spread,
- f_{yp} peak scuffing force,
- f_{zp} vertical force on tyre group,
- Δ_{ypt} percentage change in peak scuffing force of a tyre configuration t relative to dual 11R22.5 tyres,
- Δ_{zp} lateral load transfer expressed as a percentage of the static vertical load, and
- α_p slip angle of the tyre group on which the peak scuffing force occurred.

5.2 Simple-trailer performance maps

Figures 5.1–5.5 show the response of the tridem simple-trailer undergoing low-speed turns with a radius of 13.75 m. Figure 5.1 shows the peak vertical force as a function of the static vertical force and axle group spread. The increased peak vertical force in Figure 5.1 is caused by the lateral load transfer that results from having an elevated roll centre above the ground plane. This figure shows that the amount of lateral load transfer and the rate of lateral load transfer per static vertical load increases as the axle group spread also increases. When laden with the same static vertical load of 29.0 kN, the peak vertical force increases from 40.70 kN to 43.20 kN when the axle group spread is increased from 2.00 m to 3.00 m.

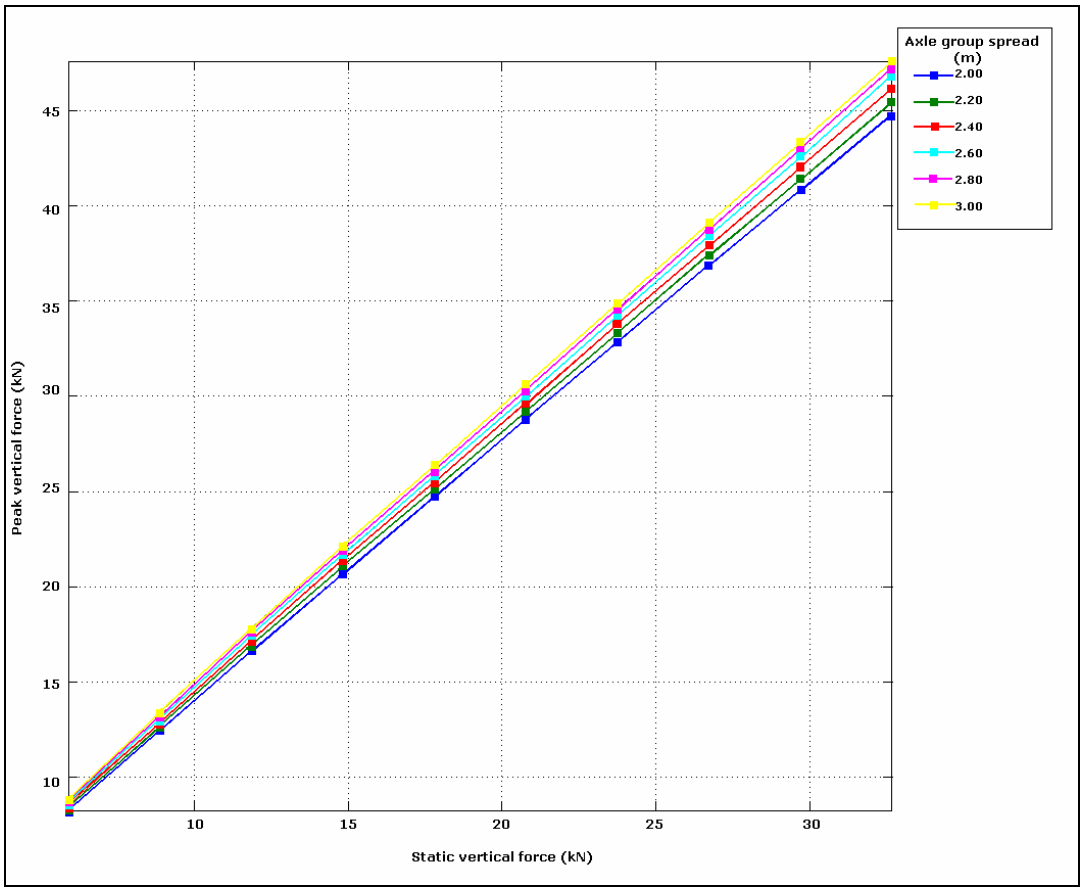

Figure 5.1 Peak vertical force v. static vertical force by axle group spread (tridem with dual 11R22.5 tyres).

Notes to Figure 5.1:
l_g = 8.50 m
r_0 = 13.75 m
Θ = 360°

Figure 5.2 gives the slip angle and Figure 5.3 gives the peak scuffing force as functions of the static vertical force and tridem axle group spread. These figures show that the slip angle and peak scuffing force increase with increasing axle group spread. When laden with the same static vertical load of 29.0 kN, the tridem axle group spread of 2.00 m generates a steady-state peak scuffing force of 24.7 kN compared with the 3.00 m spread, which generates 31.0 kN. Because of the nonlinear tyre characteristics, the peak scuffing force increases at a reducing rate with increasing axle group spread and with increasing vertical load.

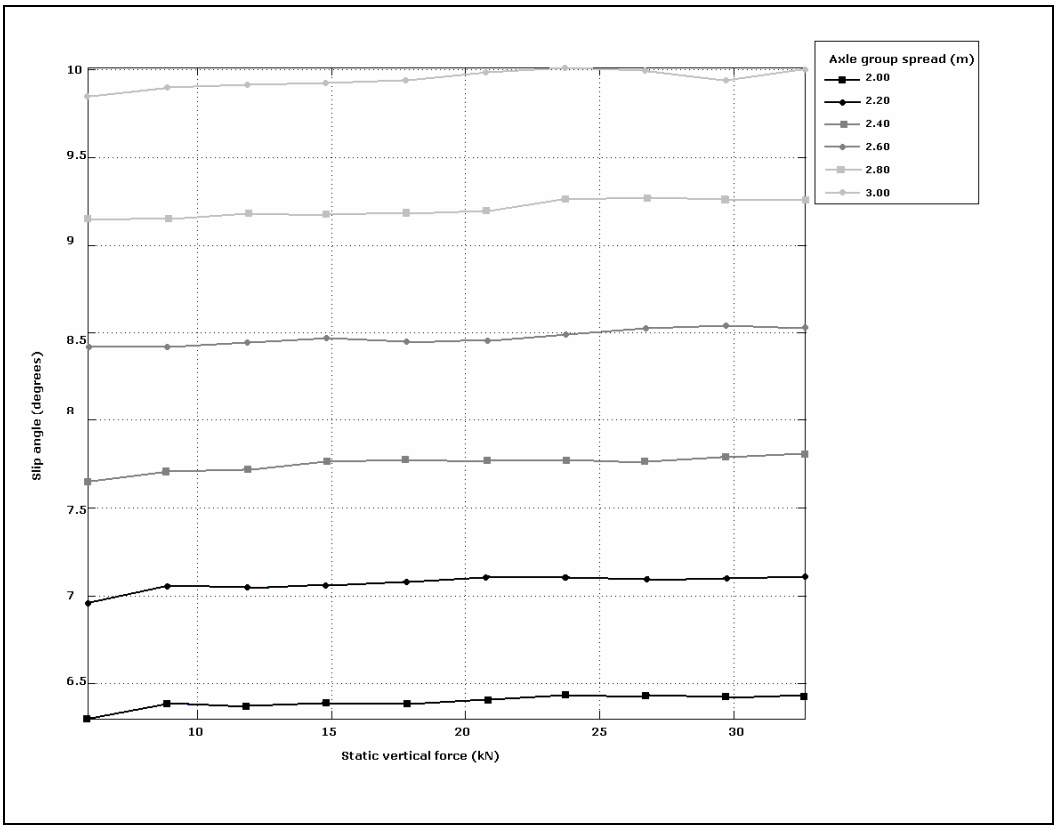

Figure 5.2 Slip angle v. static vertical force by axle group spread (tridem with dual 11R22.5 tyres).

Notes to Figure 5.2:
l_g = 8.50 m
r_0 = 13.75 m
Θ = 360°

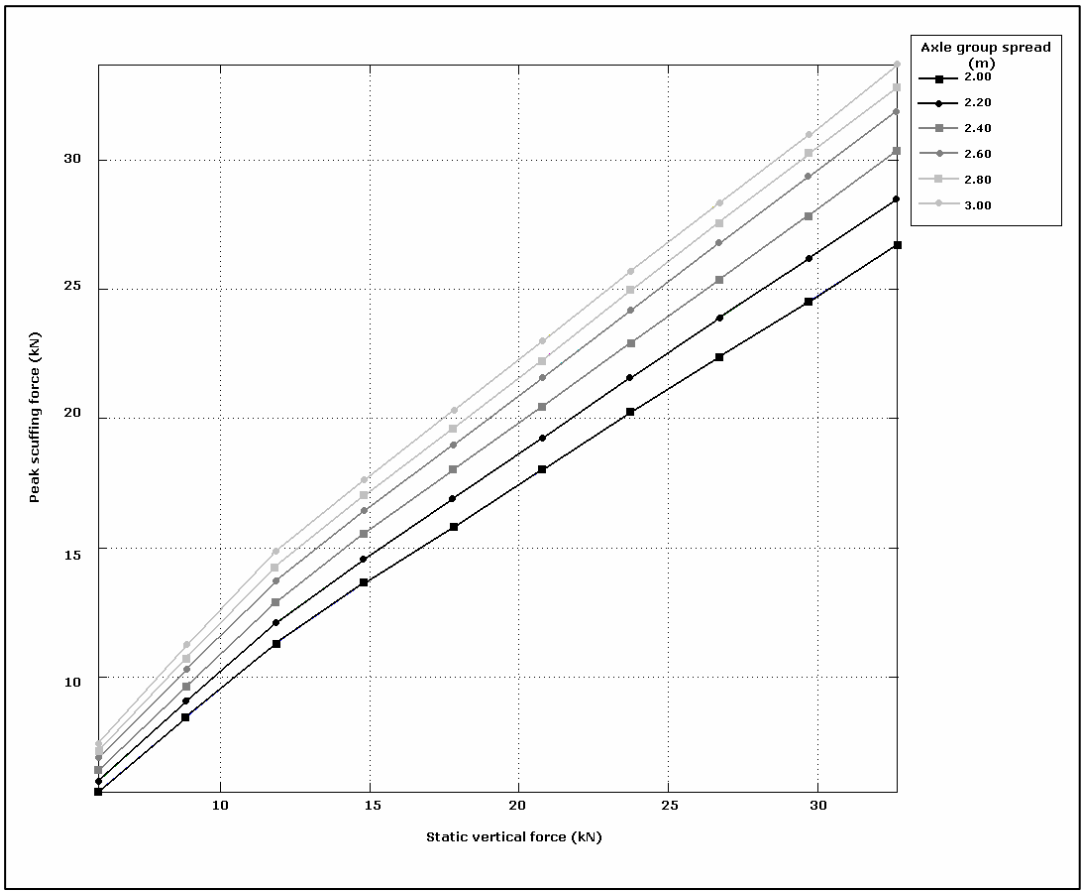

Figure 5.3 Peak scuffing force v. static vertical force by axle group spread (tridem with dual 11R22.5 tyres).

Notes to Figure 5.3:
l_g = 8.50 m
r_0 = 13.75 m
Θ = 360°

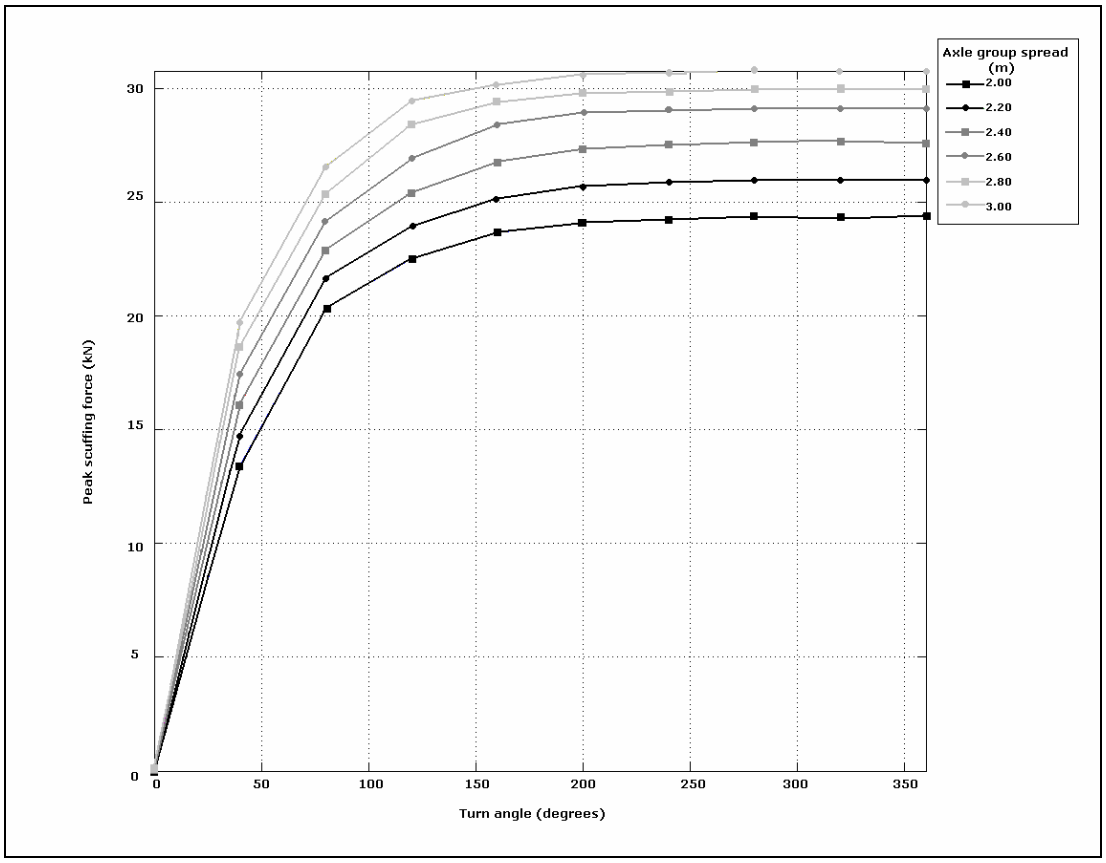

Figure 5.4 Peak scuffing force v. turn angle by axle group spread (tridem with dual 11R22.5 tyres).

Notes to Figure 5.4:
f_{z0} = 29.42 kN
l_g = 8.50 m
r_0 = 13.75 m

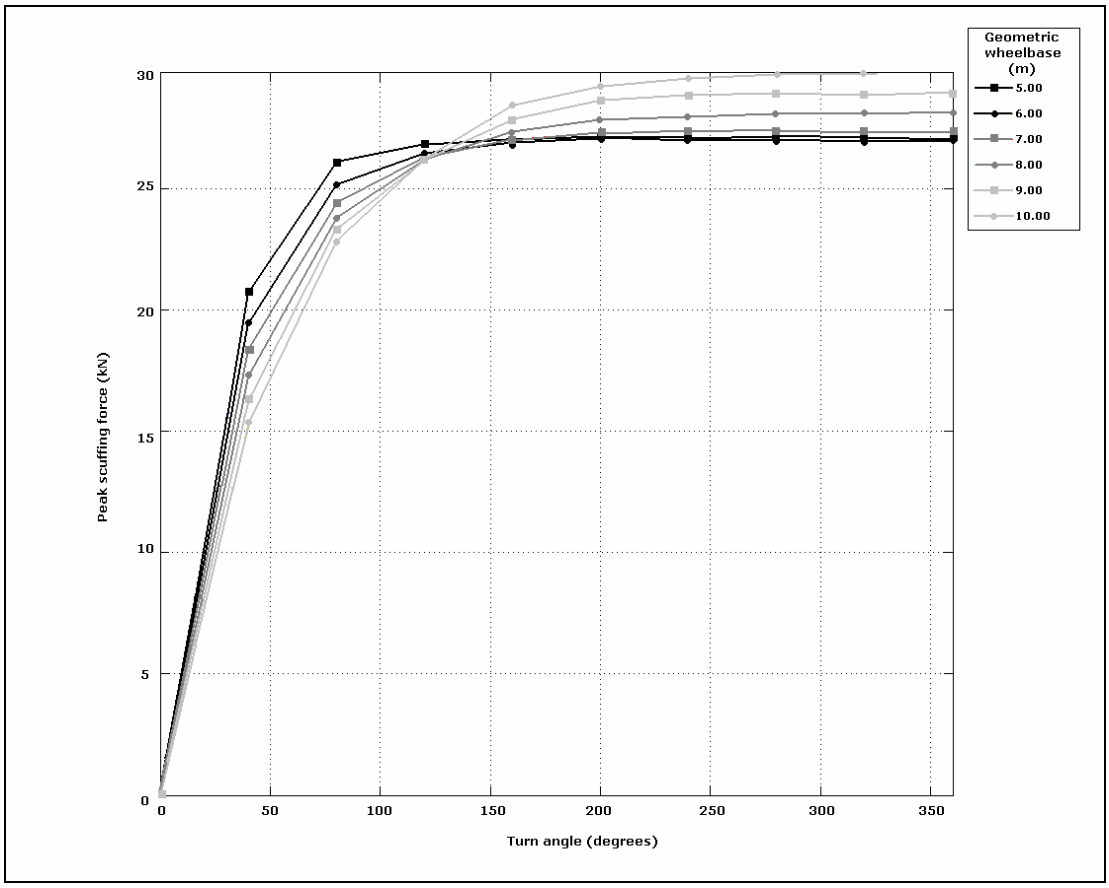

Figure 5.5 Peak scuffing force v. turn angle by geometric wheelbase (tridem with dual 11R22.5 tyres).

Notes to Figure 5.5:
f_{z0} = 29.42 kN
s = 2.50 m
r_0 = 13.75 m

Figure 5.4 gives the peak scuffing force as a function of turn angle and tridem axle group spread, and Figure 5.5 gives the peak scuffing force as a function of turn angle and geometric wheelbase. These figures show that the peak scuffing force increases with increasing turn angle, reaching a steady-state value.

Figure 5.4 shows that the peak scuffing force for wide tridem axle group spreads increases at a greater rate per angle of turn and attains a higher level of steady-state peak scuffing force than narrower spreads. Regardless of axle group spread, they achieve steady-state at approximately the same angle of turn (about 250^o).

Figure 5.5 shows that the peak scuffing forces on longer wheelbase vehicles increase at a slower rate per angle of turn than comparable vehicles with shorter wheelbases. However, the steady-state peak scuffing forces are higher for longer wheelbase vehicles than for comparable shorter wheelbase vehicles. The cross-over point occurred at about 130^o of turn angle.

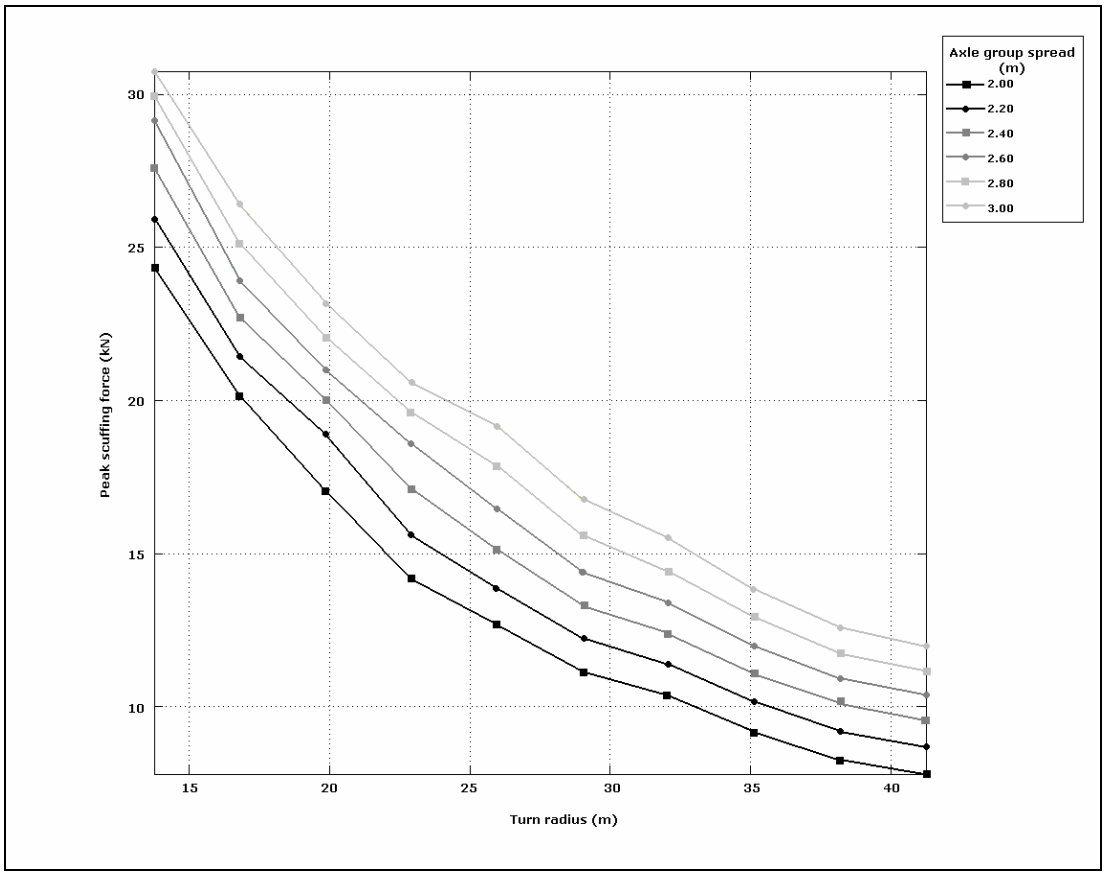

Figure 5.6 Peak scuffing force v. turn radius by axle group spread (tridem with dual 11R22.5 tyres).

Notes to Figure 5.6:
f_{z0} = 29.42 kN
l_g = 8.50 m
Θ = 360°

Figure 5.6 gives the peak scuffing force of the tridem simple-trailer undertaking 360° low-speed turns for different turn radii and axle group spreads. This figure shows that the peak scuffing force tends to zero with decreasing tridem axle group spread and with increasing turn radius.

The performance maps showing the peak scuffing force as a function of the static vertical force for both the tandem and tridem axle groups are given in Appendix B. The scuffing force calculations for the tandem axle group performance map can also be applied to tridem or quad-axle groups having two non-steering axles within the group, assuming identical equivalent wheelbases, and assuming that the self-steering axles do not reach their maximum steer angle limits and that centring force effects are negligible.

5.3 Vehicle performance maps

5.3.1 Diagrams

The graphs in this section map the performance of typical vehicle types in New Zealand fitted with 11R22.5 tyres and undergoing a 13.75 m radius low-speed turn for different angles of turn.

- Figure 5.7 gives the peak scuffing force;
- Figure 5.8 gives the peak scuffing force normalised by the vertical force or the peak scuffing force per unit vertical load;
- Figure 5.9 gives the amount of lateral load transfer expressed as a percentage of the static vertical load; and
- Figure 5.10 gives the slip angle.

Normalising the peak scuffing force by the vertical load, as shown in Figure 5.8, reduces the effect of having different axle weights and presents a clearer picture when considering equally loaded axles, and it also removes, to some extent, the effects of lateral load transfer.

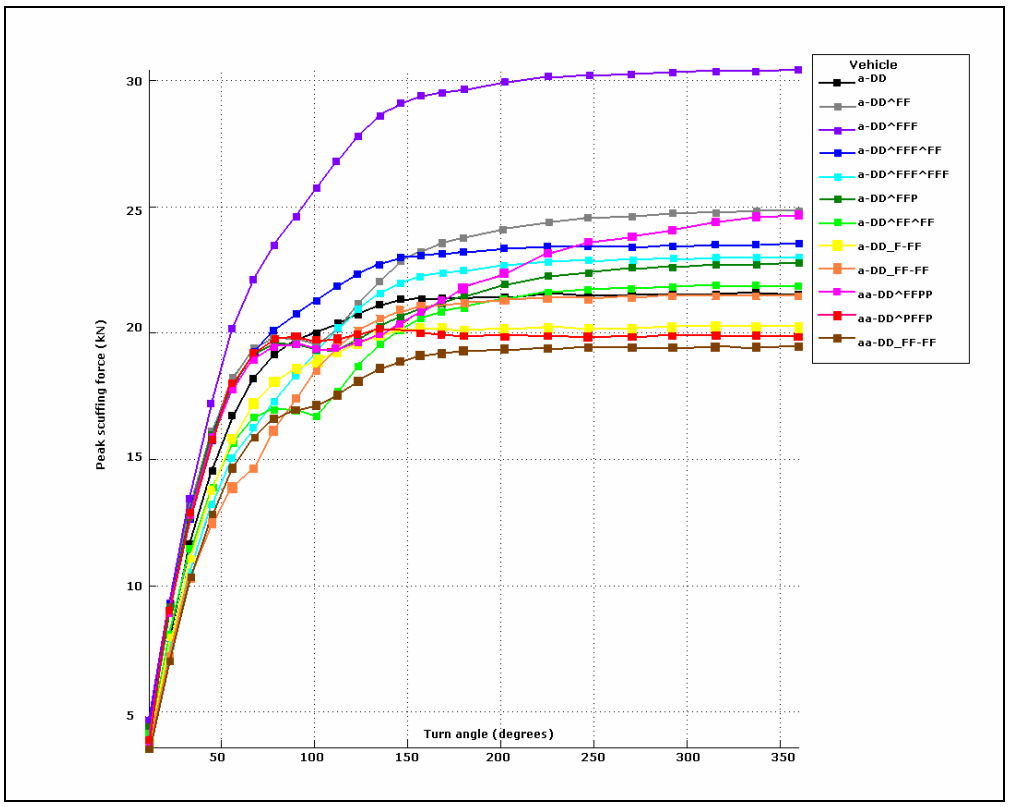

Figure 5.7 Peak scuffing force v. turn angle by vehicle type (11R22.5 tyres).

Notes to Figure 5.7:
r_0 = 13.75 m

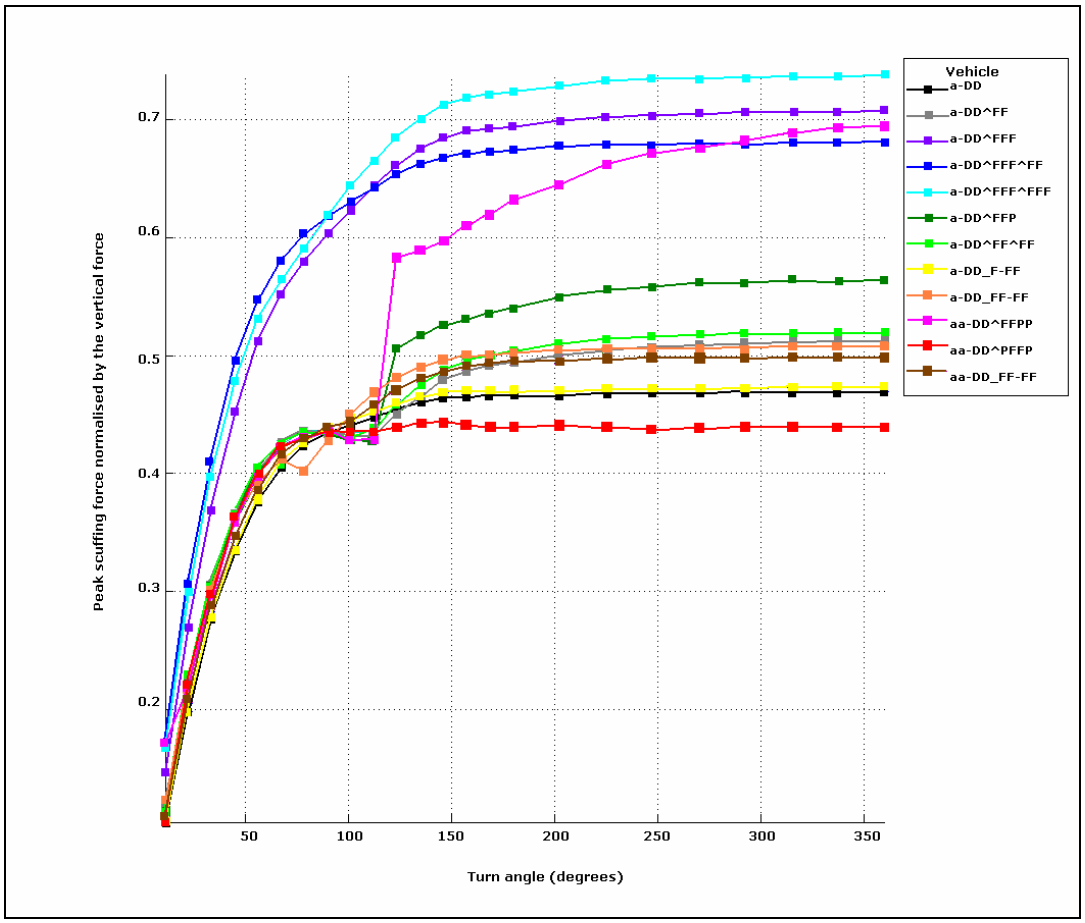

Figure 5.8 Peak scuffing force normalised by the vertical force v. turn angle by vehicle (11R22.5 tyres).

Notes to Figure 5.8:
r_0 = 13.75 m

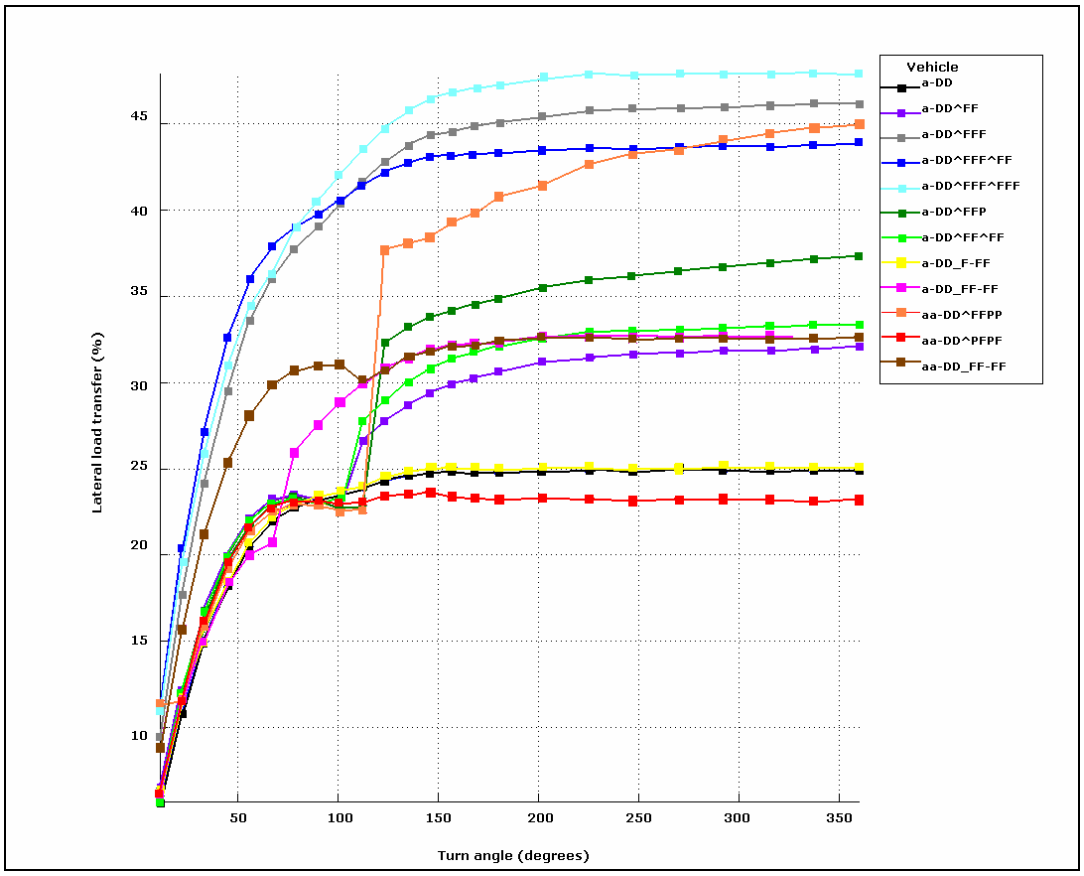

Figure 5.9 Lateral load transfer v. turn angle by vehicle type (11R22.5 tyres).

Notes to Figure 5.9:
r_0 = 13.75 m

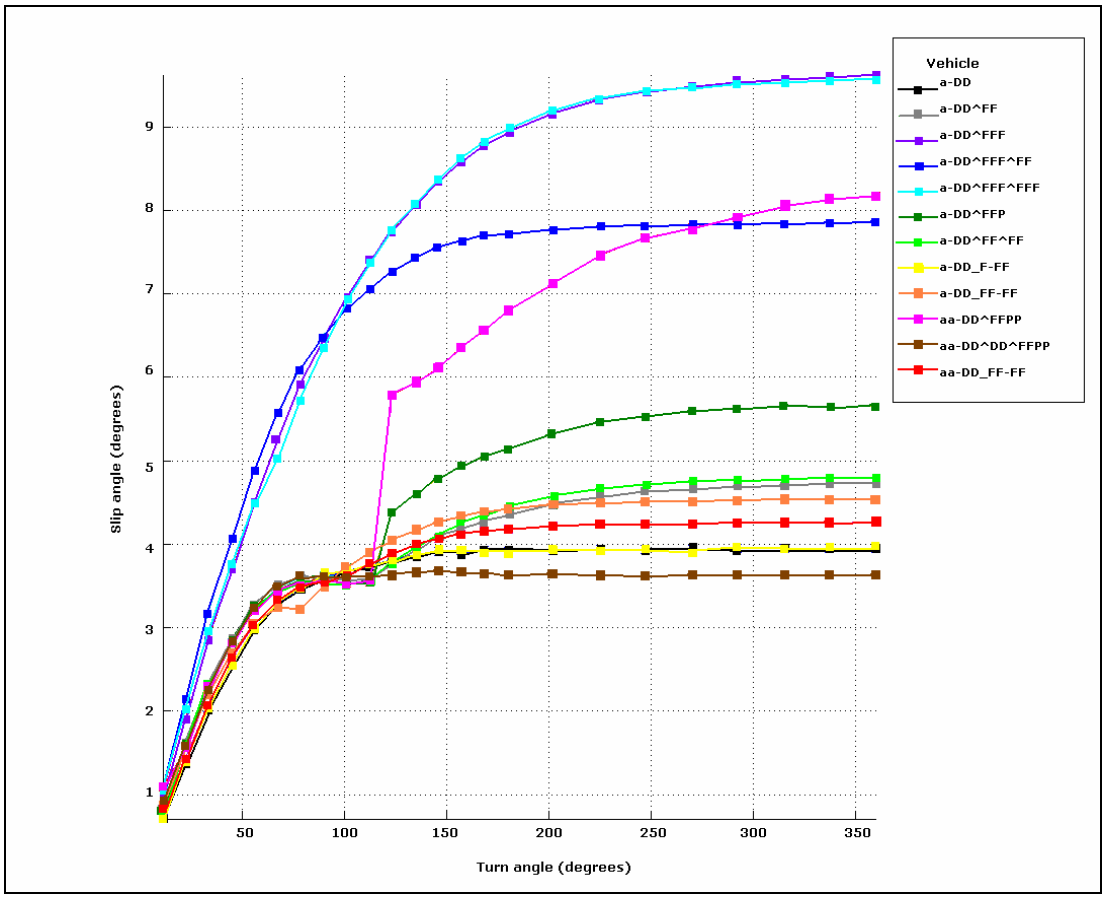

Figure 5.10 Slip angle v. turn angle by vehicle type (11R22.5 tyres).

Notes to Figure 5.10:
r_0 = 13.75 m

Table 5.1 gives the critical axle on which the peak scuffing force has occurred. For a given row, the empty boxes in Table 5.1 take on the value of the leftmost non-zero axle number.

Table 5.1 Vehicle v. peak scuffing force axle number for different angles of turn.

Vehicle	Turn angle										
	11.25°	22.50°	33.75°	45.00°	56.25°	67.50°	78.75°	90.00°	101.25°	112.50°	123.75°
a-DD	2										
a-DD^FF	2	2	2	2	2	2	2	2	2	4	
a-DD^FFF	4										
a-DD^FFF^FF	4										
a-DD^FFF^FFF	4	4	4	4	4	4	7				
a-DD^FFP	2	2	2	2	2	2	2	2	2	2	4
a-DD^FF^FF	2	2	2	2	2	2	2	2	2	6	
a-DD_F-FF	2										
a-DD_FF-FF	2	2	2	2	2	2	6				
aa-DD^FFPP	3	3	3	3	3	3	3	3	3	3	5
aa-DD^PFFP	3										
aa-DD_FF-FF	5	5	5	5	5	5	5	5	5	7	

5.3.2 Scuffing forces

The steady-state peak scuffing forces generated by vehicles without self-steering axles are presented in Table 5.2.

Table 5.2 Steady-state scuffing force generated by vehicles without self-steering axles.

Vehicle type	Level of force generated (kN)	Ranking[a]
Tractor semi-trailer	25.0–30.5	tridem semi-trailer tandem semi-trailer
B-trains	22.0–24.0	eight-axle B-train nine-axle B-train seven-axle
truck and full-trailers[b]	19.5–22.0	three-axle single-unit truck[c] seven-axle truck and full-trailer[c] eight-axle truck and full-trailer

Notes to Table 5.2:
a Vehicles are listed in descending order according to the amount of scuffing force generated.
b Included single-unit trucks.
c These two vehicles were ranked equally.

The steady-state peak scuffing forces generated by the three tractor semi-trailers with self-steering axles are between 20.0–24.5 kN, which is similar in magnitude to that generated by B-trains. The quad-semi with the twin rear-mounted self-steering axles generated the highest steady-state peak scuffing force, followed by the tridem-semi with the single rear-mounted self-steering axle, and then by the quad-semi with the front and rear-mounted self-steering axles. For these vehicles, the peak scuffing forces are similar in magnitude to each other (19.0 kN) for turn angles less than 112.5^{o}.

5.3.3 Slip angle, peak scuffing force per unit load, percentage lateral load transfer

Of the vehicles without self-steering axles, the results for the greatest slip angles, peak scuffing forces per unit load, and percentage lateral load transfers are separated distinctly into two groups depending on whether the vehicle had tridem axle groups or only tandem axle groups. The first category contains vehicles with tridem axle groups:

- the tractor semi-trailers, and
- B-trains.

The second category consisted of vehicles with tandem axle groups:

- tractor semi-trailers,
- B-trains,
- truck and full-trailers, and
- single-unit trucks.

Table 5.3 shows the slip angle, peak scuffing force per unit load and lateral load transfer during a steady-state turn for both categories.

Table 5.3 Slip angle, peak scuffing force per unit load, and lateral load transfer of the two vehicle categories.

Category	Slip angle	Peak scuffing force per unit load	Lateral load transfer
Tandem axle groups	3.9°–4.8°	0.47–0.52	25%–33%
Tridem	7.8°–9.8°	0.97–0.73	44%–47%

Of the tractor semi-trailers with self-steering axles, the slip angles, peak scuffing forces per unit load, and lateral load transfers fall into either the tandem or tridem axle group categories depending on the angle of turn. The reasons for this are discussed in Section 5.3.4.

5.3.4 Peak scuffing force and critical axle group shift

The axle group on which the peak scuffing forces occur can change as the turn angle increases. If a change occurs, in general, the critical axle group shifts backward through the vehicle's more widely spread axle groups, although not necessarily in succession. Consider the tandem-semi and the seven-axle B-train, for example. The peak scuffing force occurred on the lead drive axles for turn angles less than 101.25°, but shifted backward to the lead axle on the rearmost tandem axle group at greater angles of turn. Similar behaviour was observed with the seven-axle truck and full-trailer, with the shift occurring at a turn angle of 67.50°. The peak scuffing force of the eight-axle truck and full-trailer occurred on the lead axle of the dolly's tandem axle group for turn angles less than 101.25°, but shifted to the lead axle of the rearmost tandem axle group for greater angles of turn. In the case of the tridem-semi and the eight-axle B-train, the peak scuffing force occurred on the lead axle of the tridem axle group for all angles of turn. Thus the tridem axle groups dominated tandem axle groups in terms of peak scuffing forces even though the tridem axle groups had less weight per axle. In the case of the nine-axle B-train, the peak scuffing force occurred on the lead axle of the lead tridem axle group for turn angles less than 67.50°, but shifted to the lead axle of the rearmost tridem axle group for greater angles of turn. For the six-axle truck and full-trailer, and the single-unit truck, the peak scuffing force occurred on the lead axles of the tandem-drive groups for all angles of turn.

The scuffing forces generated by self-steering axle groups depend on the number and distribution of self-steering axles, the centring force characteristics, and on the maximum steer angles permitted. For large angles of turn, the axles can reach their steer angle limits, at which point they respond like non-steering axles. These characteristics can affect the location of the equivalent single axle, the equivalent wheelbase, the axle group spread, and ultimately the peak scuffing forces. For example, the peak scuffing forces for all three vehicles were similar in magnitude (19.0 kN) for turn angles less than 112.5°; this scuffing occurred on the lead drive axles. For greater angles of turn, the quad-semi with the twin rear-mounted self-steering axles showed an increase in peak scuffing forces and, to a lesser extent, so did the tridem-semi with the single rear-mounted self-steering axle. At these increased angles of turn, the self-steering axles reach their maximum steer angle limits and these axles respond like non-steering axles. This results in increasing

peak scuffing forces and in increasing peak scuffing forces per unit load until steady-state is reached. However, the self-steering axles on the quad-semi with the front and rear-mounted self-steering axles never reached their maximum steer angle limits for all angles of turn, and thus had the least amount of peak scuffing force for this type of vehicle. The peak scuffing forces for this vehicle remained on the lead drive axle for all angles of turn.

5.3.5 Tyre size, dual tyre and wide-single tyres

Table 5.4 shows the effects of having different tyre configurations on the trailers of the four reference vehicles undergoing a 360° steady-state low-speed turn with a modest turn radius of 18.75 m. The 11R22.5 and 245/70R19.5 tyres are in dual configuration, and the 385/65R22.5 tyres are configured as wide-singles. Single and dual 11R22.5 tyres are used on the steer and drive axles of all of the powered units in this analysis. Note the axle number and the relative magnitudes of the peak slip angles on which the peak scuffing force has occurred for the different vehicles.

Table 5.4 Effects of different trailer tyres on the reference vehicles undergoing a 360° steady-state turn at a radius of 18.75 m.

Tyres	Reference vehicle	f_{vp} (kN)	f_{zp} (kN)	$\frac{f_{vp}}{f_{zp}}$	Δ_{vpt} (%)	Δ_{zp} (%)	α_p (deg)	Axle
11R22.5	aa-DD_FF-FF	13.2	36.4	0.362	0	24	2.8	7
245/70R19.5	aa-DD_FF-FF	12.9	35.3	0.366	-2	20	2.8	7
385/65R22.5	aa-DD_ff-ff	13.1	35.6	0.367	-1	21	2.8	7
11R22.5	a-DD^FFF^FF	18.1	32.7	0.554	0	36	5.2	4
245/70R19.5	a-DD^FFF^FF	18.5	31.6	0.584	2	32	5.2	4
385/65R22.5	a-DD^fff^ff	20.1	32.3	0.622	11	35	5.2	4
11R22.5	a-DD^FFF	22.8	40.3	0.567	0	37	5.7	4
245/70R19.5	a-DD^FFF	23.8	39.1	0.608	4	33	5.7	4
385/65R22.5	a-DD^fff	26.1	40.1	0.651	14	36	5.7	4
11R22.5	aa-DD^FFPP	17.1	33.1	0.518	0	35	4.4	5
245/70R19.5	aa-DD^FFPP	17.1	31.6	0.541	0	29	4.6	5
385/65R22.5	aa-DD^ffpp	17.0	31.9	0.534	-1	30	4.2	5

Relative to the dual 11R22.5 tyre configuration, the greatest increase in steady-state peak scuffing forces occurred on tridem axle groups configured with 385/65R22.5 wide-single tyres, with the tridem-semi experiencing a 14% increase and the seven-axle B-train experiencing an 11% increase. When configured with dual 245/70R19.5 tyres, the tridem-semi generates a 4% increase in steady-state peak scuffing force relative to the dual 11R22.5 tyre configuration, and the seven-axle B-train generates a 2% increase. The changes in peak scuffing force for the remaining vehicles are less significant by comparison.

Relative to the dual 11R22.5 tyre configuration, the greatest reduction in lateral load transfer occurred on the vehicles fitted with dual 245/70R19.5 tyres, with the quad-semi experiencing a 6% reduction. The remaining vehicles show a 4% reduction in lateral load transfer when fitted with dual 245/70R19.5 tyres. When fitted with 385/65R22.5 wide-single tyres, the quad-semi shows a 5% reduction in lateral load transfer relative to the dual 11R22.5 tyre configuration, and the eight-axle truck and full-trailer shows a 3% reduction. The changes in lateral load transfer for the remaining vehicles are less significant in comparison.

6. Discussion

To recap the findings of the previous chapter, for a given tyre and horizontal pavement surface, the magnitude of the cornering or scuffing force increases with slip angle and with vertical load. For small slip angles, the cornering force increases linearly with slip angle. For larger slip angles, the cornering force increases nonlinearly with slip angle at a reducing rate. The cornering force also increases nonlinearly with vertical load at a reducing rate.

A number of findings relate to the impact of vehicle and turn parameters on the magnitude of the peak scuffing forces generated by multi-axle groups during constant low-speed turns.

- **Axle groups with self-steering axles generate lower scuffing forces than comparable non-steering axle groups.** This outcome is the main motivation behind having self-steering axles. The peak scuffing forces generated by self-steering axle groups depend on the number and distribution of self-steering axles, on the centring force characteristics, and on the maximum steer angles permitted. For tight turns, however, these axles can reach their steer angle limit, at which point they respond like non-steering axles and thus giving rise to an increase in scuffing forces. Of the self-steering tractor semi-trailers undergoing the 13.75 m radius turn, the quad-semi with the twin rear-mounted self-steering axles generated the highest steady-state peak scuffing forces, followed by the tridem-semi with the single rear-mounted self-steering axle, and then by the quad-semi with the front and rear-mounted self-steering axles. But for turn angles less than 112.5^{o}, the peak scuffing forces are similar in magnitude to each other (19.0 kN) and occurred on the lead drive axles. For most on-road low-speed turns, the effects on pavement surface wear from each of these vehicles are very similar.
- **For the same axle group weight and axle group spread, wide-single tyres generate higher scuffing forces than dual tyres.** When undergoing the modest 18.75 m radius turn, the tridem-semi generated a 14% increase in steady-state peak scuffing force when fitted with 385/65R22.5 tyres (26.1 kN) compared to when fitted with dual 11R22.5 tyres (22.8 kN). When fitted with dual 245/70R19.5 tyres, the same tridem axle group generated a 4% increase in steady-state peak scuffing force compared to dual 11R22.5 tyres. This result is consistent with the relative amount of cornering force produced by this particular tyre configuration. The corresponding lateral load transfers are shown to increase above the static weight by 4% when changing from dual 245/70R19.5 to dual 11R22.5 tyres, and by 1% when changing from 385/65R22.5 wide-singles to dual 11R22.5 tyres. These results are consistent with increasing roll centre and sprung mass CG heights and with reducing tyre track widths, respectively.

- **Scuffing forces increase with increasing axle group spread.** Increasing axle group spread increases an axle's longitudinal distance from the equivalent single axle. Increasing this distance increases the curvature of the path and slip angle experienced by the corresponding tyres. These increases result in increasing lateral load transfers and scuffing forces.
- **When laden to the maximum legal weight limits, tridem axle groups produce higher scuffing forces than tandem axle groups even though the tridem axle groups have less weight per axle.** At legal axle group weight limits, tridem axles weigh 6 tonnes each while tandem axles weigh 7.5 tonnes each. Even with this weight difference, tridem axle groups generate higher scuffing forces than tandems. At these weights and when configured with dual 11R22.5 tyres, the tridem axle group generated 30.5 kN, which equates to 22% more steady-state peak scuffing than the tandem axle group (25.0 kN) when undergoing the 13.75 m radius turn. The corresponding load transfers are 32% and 46% above the static vertical loads for the tandem and tridem axle groups, respectively. The increased scuffing force results from the differences in axle group spreads, lateral load transfers, and from the nonlinear tyre characteristics. The axle group spreads were 1.35m and 2.70m for the tandem and tridem axle groups, respectively.
- **Scuffing forces decrease with increasing turn radius.** This result is consistent with the decreasing curvature of the path or with the increasing radius of curvature experienced by the axle group.
- **For vehicles without self-steering axles, the highest steady-state scuffing forces are generated by tractor semi-trailers, followed by B-trains, then truck and full-trailers, and then single-unit trucks.** When undergoing the 13.75 m radius turn, the steady-state peak scuffing forces generated by the tractor semi-trailers, B-trains, and truck and full-trailers (including single-unit trucks) ranged from 25.0–30.5 kN, 22.0–24.0 kN, and 19.5–22.0 kN, respectively. One reason for this is that tractor semi-trailers are laden with higher loads for a given axle group configuration than other vehicles of similar length. A second reason is that the rear axle groups on tractor semi-trailers experience greater levels of curvature during a steady-state turn than other vehicles of similar length. A third reason is that axle groups with more axles have wider axle spreads, so vehicles with tridem axle groups generate higher scuffing forces and lateral load transfers than vehicles with only tandem axle groups.
- **Even during low-speed turns with minimal lateral acceleration, significant lateral load transfer can occur from having an elevated roll centre, thus leading to higher peak vertical loads.** The result is that higher peak scuffing forces occur than would be the case if no load transfer took place. For a legally configured tridem-semi undergoing a 13.75 m radius 90^{o} turn, this lateral load transfer can increase the peak vertical load by up to 40% above the static load. The mechanism responsible for this lateral load transfer depends on axle group spread and on the roll centre height of the suspension. The tyre-spread across the axle group induces transverse shear forces that act at the

pavement–tyre interface. Since the roll centre of the suspension is some distance above the ground plane, a roll moment is induced at the roll centre. To maintain a moment balance about the roll centre, load must be transferred laterally from one side of an axle to the other. Lateral load transfer caused by body roll can also be induced by tow coupling forces applied at a vertical distance offset from the roll centre but this effect is only significant for large articulation angles. No lateral load transfer caused by body roll will occur if the tow coupling is at the same height as the roll centre of the suspension.

- **For small angles of turn (90^o or less), shorter wheelbase single-unit vehicles generate higher scuffing forces than comparable vehicles with longer wheelbases but the reverse is true for large turn angles as these vehicles approach steady-state.** This is because, for a given turn radius, the maximum scuffing forces occur at steady-state when the curvature of the axle groups are maximal. In steady-state, the axle groups on shorter wheelbase vehicles experience lower levels of curvature than comparable vehicles with longer wheelbases, but shorter wheelbase vehicles require smaller angles of turn to reach steady-state than comparable vehicles with longer wheelbases.
- **For a given turn radius, the axle group on which the peak scuffing forces occur can change as the turn angle increases.** If a change occurs, in general, the critical axle group shifts backward through the vehicle's more widely spread axle groups, although not necessarily in succession. This results from the differences in axle group spreads, static axle weights, and lateral load transfers, and on the curvature of the path of the axle group. To achieve a cornering force balance, the peak scuffing forces generally occurs on the tyres of the lead non-steering axle within the axle group.
- **Minor visible abrasion of the chipseal surface was observed in the field trial at the lowest gross tandem axle group load, which was a little under 7 tonnes.** Small fragments approximately 1 mm in diameter were broken off the exposed corners of the chip. Based on the computer simulation, this damage resulted from a peak scuffing force of a least 33.2 kN. A peak scuffing force of 30.5 kN was calculated for a legally configured tridem semi-trailer undergoing the 13.75 m radius 360^o turn. This latter manoeuvre is less severe than the 25 m wall-to-wall 360^o turn capability required by the VDM Rule.

7. Conclusions

7.1 Key findings

It is clear from the study that reducing axle weight, axle group spread, and road curvature (increasing turn radius) reduces scuffing forces and their impact on pavement wear. The amount of scuffing force also depends on the tyre configuration, the use of self-steering axles, and on the type of vehicle.

A rule-of-thumb observation which was given in Fancher & Winkler (2007) and is also conveyed in this study is that:

> *…what one does to improve low speed performance is likely to degrade high speed performance and vice versa.*

For example, wide-single tyres produce higher scuffing forces than dual tyres. However, the use of wide-single tyres increases the tyre track width, which can slightly improve rollover stability. The use of self-steering axles results in lower scuffing forces but the lower overall cornering stiffness reduces high-speed directional performance compared with non-steering axle groups. For vehicles without self-steering axles, the highest steady-state scuffing forces are generated by tractor semi-trailers, followed by B-trains, and then truck and full-trailers. This ranking of heavy vehicles is similar to that when ranked, in descending order, of high-speed directional performance.

The tyre cornering stiffness, and therefore the amount of scuffing force, also depends on inflation pressure. In the case of truck tyres, the influence of inflation on cornering stiffness varies and depends on obscure sensitivities to details in the carcass design. Therefore, the overall influence of inflation pressure on cornering stiffness cannot be generalised across all tyre types.

In general, the pavement wear resulting from scuffing forces will depend on many factors including the overall pavement design and the condition of the pavement, and on various environmental factors.

7.2 Recommendations

- When designing intersections and roundabouts, the turn radius should be as large as possible. This will lead to reduced scuffing forces.
- Where tight radius turns are unavoidable, the pavement surface design should take into account the high levels of scuffing forces that will occur.
- Research should be undertaken to determine whether the weight limits on tridem and quad-axle groups should vary with dual or wide-single tyre configurations. The VDM Rule allows for tandem axle groups to carry more weight when configured with dual tyres than they can with wide-single tyres. The VDM Rule for tridem and quad-axle groups permits the same axle weight limit regardless of tyre configuration.
- Research should be undertaken to investigate whether a pavement scuffing force damage component should be incorporated into the Road User Charges Cost Allocation Model. The current Cost Allocation Model accounts for the pavement wear caused by vertical loads but does not account for the impact of pavement scuffing forces on pavement wear for a given vehicle configuration.

8. References

AUSTROADS. 1995. *Guide to Traffic Engineering Practice Intersections at Grade Part 5.* Granville, Australia: Ambassador Press Pty. 67 pp.

Fancher, P.S., Ervin, R.D., Winkler, C.B., Gillespie, T.D. 1986. *A Factbook of the Mechanical Properties of the Components for Single-Unit and Articulated Heavy Trucks.* Washington DC: U.S. Department of Transportation. 184 pp.

Fancher, P., Winkler, C. 2007. Directional performance issues in evaluation and design of articulated heavy vehicles. *International Journal of Vehicle Mechanics and Mobility, Vehicle System Dynamics, Vol. 45, No. 7–8, July–August 2007*: 607–647.

Gillespie, T.D., MacAdam, C.C. 1982. *Constant Velocity Yaw/Roll Program User's Manual*. Ann Arbor, Michigan, United States of America: The University of Michigan Transportation Research Institute. 117 pp.

Gillespie, T.D. 1992. *Fundamentals of Vehicle Dynamics.* Warrendale, Pennsylvania: Society of Automotive Engineers, Inc. 471 pp.

Jacobs, M.M.L., Moraal, J. 1992. The influence of tire characteristics on normal stresses in asphalt concrete pavements. Pp 218–224 in *Third International Symposium on Heavy Vehicle Weights and Dimensions, Cambridge, UK, 28 June–2 July, 1992*.

Latto, D., Baas, C. 2002. *Quad-axle Semi Trailer – Field Trial. July 2002.* TERNZ report. Auckland, New Zealand: TERNZ. 41 pp.

LTSA. 2002. *Land Transport Rule: Vehicle Dimensions and Mass 2002 – Rule 41001.* Wellington: Land Transport Safety Authority (LTSA). 117 pp.

LTNZ. 2007. *Land Transport Rule: Vehicle Dimensions and Mass Amendment (No 2) 2007 – Rule 41001/3.* Wellington: Land Transport New Zealand (LTNZ).

National Transport Commission. 2006. *Administrative Guidelines, Rules and Codes for Operation of Performance Based Standards Vehicles. The Standards and Rules for Assessment of Potential Performance Based Standards Vehicles (Version 1.1).* Melbourne: National Transport Commission. 137 pp.

UMTRI. 2000. The mechanics of heavy-duty trucks and truck combinations. *Engineering Summer Conference. The University of Michigan Transportation Research Institute (UMTRI). Summer 2000. Volume 2.*

Appendix A Model properties

Tables A1–A4 give the tyre properties, relevant suspension parameters, and the coupling and sprung mass CG heights used in the study. These are based on the values from the VDM Rule and from Fancher et al. (1986).

Table A1 Tyre properties.

Parameter	Vertical stiffness (kN/m)	Rolling radius (m)	Width (m)	Dual spacing (m)
255/70R22.5 (field trial)	874.2332	0.490	0.279	0.300
11R22.5	874.2332	0.490	0.279	0.300
245/70R19.5	874.2332	0.400	0.248	0.280
385/65R22.5	1049.0798	0.490	0.387	0.000

Table A2 Relevant trailer suspension parameters.

Parameter	Unit	Steer axle ERF[c] OEM[c] steel-leaf	Drive axle DAF[c] 85CF OEM[c] steel-leaf	Trailer axle Hutch 9600 steel-leaf	Trailer axle Hutch 9700 (field trial)
Auxiliary roll stiffness	Nm/rad	24 800	41 417	38 841	38 841
Overall mass[a]	kg	544	1043	798	798
CG height	m	rr[b]	rr	rr	0.49
Roll centre height	m	rr-0.02	rr+0.2	rr+0.2	0.69
Suspension track width	m	0.80	0.97	0.97	0.97
Overall tyre track width	m	2.3	2.4	2.4	2.4

Notes to Table A2:
a Overall mass = axle mass + tyre masses
b rr = rolling radius of tyre.
c Manufacturers' names

Table A3 Coupling and sprung mass CG heights for the vehicle models.

Parameter	Value (m)
Fifth wheel coupling height	1.35
Tow-eye coupling height	0.94
Turntable coupling height	1.25
Tractor sprung mass CG height	1.12
Trailer sprung mass CG height	rr*+1.76
Truck sprung mass CG height	rr+1.61

* rr = rolling radius of tyre.

Table A4 Coupling and sprung mass CG heights for the simple-trailer models (including field trial).

Parameter	Value (m)
Tow-eye coupling height	0.69
Trailer sprung mass CG height	rr*+1.76

***** rr = rolling radius of tyre.

The relevant vehicle parameters are shown in Table A5. 'Unit wheelbase' corresponds to the nominal wheelbase as specified in the VDM Rule, i.e. the length from the front axis to the rear axis. 'Unit coupling offset' is the displacement of the coupling from the rear axis. By convention, a positive value indicates a displacement forward of this axis, while a negative sign denotes a backward displacement.

Table A5 Parameters of the vehicles used in the computer model.

Tyre and axle coupling sequence unit	Unit wheelbase (m)	Unit coupling offset (m)	Axle group spread (m)	Axle group gross mass (kg)
a-DD	5.875	0	0 1.35	6000 15 000
a-DD^FF	4.25 8.5	0.275	0 1.35 1.35	6000 15 000 15 000
a-DD^FFF & a-DD^fff	4.25 8.5	0.275	0 1.35 2.7	6000 15 000 18 000
a-DD^FFP	4.25 8.5	0.275	0 1.35 2.7	6000 15 000 18 000
aa-DD^FFPP & aa-DD^ffpp	5.15 8.5	0.70	1.72 1.35 4	9000 15 000 20 000
aa-DD^PFFP	5.15 8.5	0.70	1.72 1.35 4	9000 15 000 20 000
a-DD^FF^FF	4.25 6.5 5.4	0.218–0.675	0 1.35 1.35 1.35	5300 12 900 12 900 12 900
a-DD^FFF^FF & a-DD^fff^ff	4.25 6.5 5.4	0.218–1.35	0 1.35 2.7 1.35	5300 12 000 14 700 12 000
a-DD^FFF^FFF	4.25 6.5 5.4	0.218–1.35	0 1.35 2.7 2.7	5300 12 900 12 900 12 900
a-DD_F-FF	5.875 3.007 5.5	-2.2 0	0 1.35 0 1.35	6000 14 000 8000 14 000
a-DD_FF-FF	4.3 5.5 4.0	-1.72 0	0 1.35 1.35 1.35	6000 12 000 13 000 13 000
aa-DD_FF-FF & aa-DD_ff-ff	5.875 3.007 5.5	-2.2 0	1.72 1.35 1.35 1.35	8000 12 000 12 000 12 000

Appendix B Tandem and tridem simple-trailer performance maps

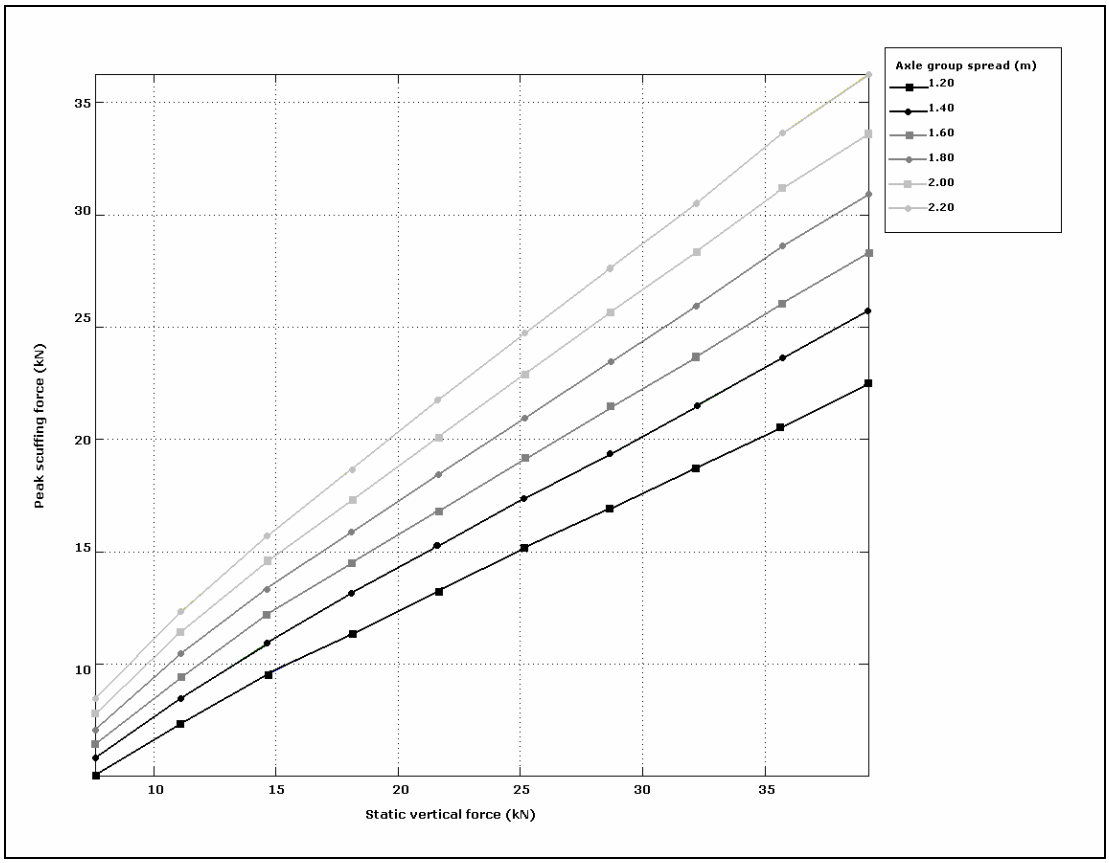

Figure B1 Peak scuffing force v. static vertical force by axle group spread (tandem with dual 11R22.5 tyres)

Notes to Figure B1:
l_g = 8.50 m
r_0 = 13.75 m
Θ= 360°
μ_p = 1.0.

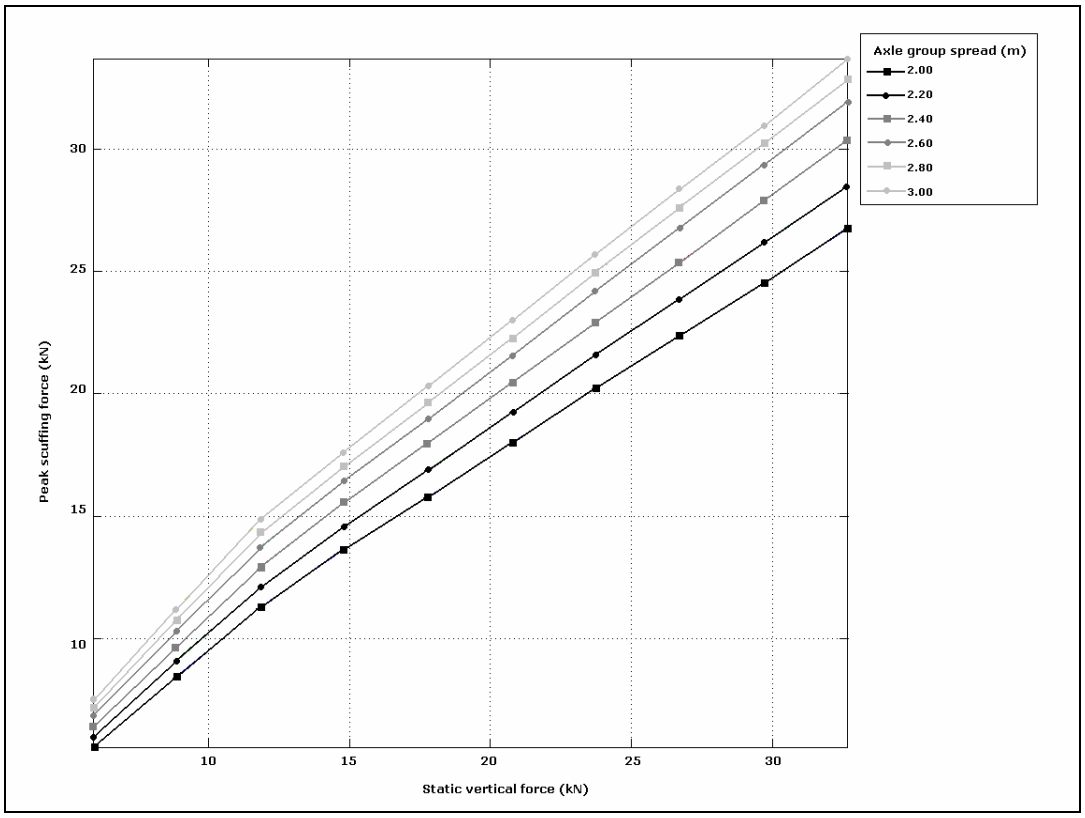

Figure B1 Peak scuffing force v. static vertical force by axle group spread (tridem, dual 11R22.5 tyres).

Notes to Figure B2:
l_g = 8.50 m
r_0 = 13.75 m
Θ= 360°
μ_p = 1.0.

Appendix C Glossary

C1 Cornering force parameters

i	axle number
j	j^{th} non-steering axle group belonging to the j^{th} vehicle unit
k	k^{th} vehicle unit
f_y	tyre cornering force or pavement scuffing force
f_z	vertical force
α	slip angle
c_α	cornering stiffness (linear tyre model used for small slip angles only)
μ_{ys}	transverse pavement–tyre static friction coefficient
μ_{yk}	transverse pavement–tyre kinetic or sliding friction coefficient
δ_{ij}	displacement from the j^{th} rear axis to the i^{th} axle (positive distance forward, negative distance rearward)
ε	distance from the rear axis to the equivalent single axle
r	radius of curvature or instantaneous turn radius of the path followed by the equivalent single axle
r_0	reference turn radius or radius of curvature of the turn
l_e	equivalent wheelbase: distance from the front axis to the equivalent single axle
l_g	geometric wheelbase: distance from the front axis to the rear axis
h	distance from the tow coupling to the corresponding equivalent single axle
N	number of non-steering axles
LSO	low-speed steady-state offtracking

C2 Lateral load transfer parameters

f_{zr}	vertical force on the right tyre group
f_{zl}	vertical force on the left tyre group
f_{yb}	lateral body force acting on the sprung mass
f_{ys}	lateral surface force applied to the sprung mass
t_t	tyre track width
h_{rc}	roll centre height above the ground plane
k_c	composite roll stiffness
Φ	body roll angle relative to the vertical axis

C3 Field trial parameters

f_{yt} peak kinetic towing force (vector)
f_{z0} static vertical load per tyre group (vector)
f_{ya} average kinetic scuffing force per tyre group (vector)
f_{yd} drag force of dolly
l_e equivalent wheelbase of 6.15 m
s tandem axle group spread of 1.35 m
μ_{yk} transverse coefficient of kinetic friction

C4 Performance map parameters

Δ_{zp} lateral load transfer expressed as a percentage of the static vertical load
f_{zp} vertical force on tyre group
f_{z0} static vertical force on tyre group
Δ_{ypt} percentage change in peak scuffing force of tyre configuration t relative to dual 11R22.5 tyres
Θ turn angle
f_{yp0} peak scuffing force of dual 11R22.5 tyres
f_{ypt} peak scuffing force of tyre configuration t
t tyre configuration: dual 11R22.5, dual 245/70R19.5, or wide-single 385/65R22.5 tyres

C5 Units of measurement

Hz Hertz (cycles per second)
k kilo (one thousand times more)
kg kilogram
km/h kilometres per hour
m metre
mm millimetre
N Newton
psi pounds per square inch
rad radian
s seconds
° degrees (deg)
^{o}C degrees Celsius

Characterising Pavement Surface Damage Caused by Tyre Scuffing Forces

Land Transport New Zealand
Research Report 347